

19th Paper_Nurhasni Hasan_Biomacromolecules (2020).pdf *by*

Submission date: 14-May-2023 09:24AM (UTC+0700)

Submission ID: 2092390684

File name: 19th Paper_Nurhasni Hasan_Biomacromolecules (2020).pdf (1.44M)

Word count: 13008

Character count: 60264

Article

Curcumin nanocrystal/pH-responsive polyelectrolyte multilayer core-shell nanoparticles for inflammation-targeted alleviation of ulcerative colitis

Murtada A. Oshi, Juho Lee, Muhammad Naeem, Nurhasni Hasan,
Jihyun Kim, Hak Jin Kim, Eun Hee Lee, Yunjin Jung, and Jin-Wook Yoo

Biomacromolecules, Just Accepted Manuscript • DOI: 10.1021/acs.biomac.0c00589 • Publication Date (Web): 23 Jul 2020

Downloaded from pubs.acs.org on July 23, 2020

Just Accepted

"Just Accepted" manuscripts have been peer-reviewed and accepted for publication. They are posted online prior to technical editing, formatting for publication and author proofing. The American Chemical Society provides "Just Accepted" as a service to the research community to expedite the dissemination of scientific material as soon as possible after acceptance. "Just Accepted" manuscripts appear in full in PDF format accompanied by an HTML abstract. "Just Accepted" manuscripts have been fully peer reviewed, but should not be considered the official version of record. They are citable by the Digital Object Identifier (DOI®). "Just Accepted" is an optional service offered to authors. Therefore, the "Just Accepted" Web site may not include all articles that will be published in the journal. After a manuscript is technically edited and formatted, it will be removed from the "Just Accepted" Web site and published as an ASAP article. Note that technical editing may introduce minor changes to the manuscript text and/or graphics which could affect content, and all legal disclaimers and ethical guidelines that apply to the journal pertain. ACS cannot be held responsible for errors or consequences arising from the use of information contained in these "Just Accepted" manuscripts.

1
2
3
4
5
6
7 1 Curcumin Nanocrystal/pH-Responsive
8
9
10
11 2 Polyelectrolyte Multilayer Core-Shell Nanoparticles
12
13
14
15 3 for Inflammation-Targeted Alleviation of Ulcerative
16
17
18
19 4 Colitis

23 5 *Murtada A. Oshi,^a Juho Lee,^a Muhammad Naeem,^a Nurhasni Hasan,^a Jihyun Kim,^{a,b} Hak Jin*

26 6 *Kim,^c Eun Hee Lee,^d Yunjin Jung,^a and Jin-Wook Yoo^{a*}*

29 7 ^a College of Pharmacy, Pusan National University, Busan, South Korea

31 8 ^b Department of Cogno-Mechatronics Engineering, College of Nanoscience & Nanotechnology,
32
33 9 Pusan National University, Busan, South Korea

36 10 ^c Department of Radiology, Pusan National University Hospital, Pusan National University
37
38 11 School of Medicine, ¹⁰ Busan, South Korea

40 12 ^d College of Pharmacy, Korea University, Sejong, South Korea

43
44
45 14 **ABSTRACT**

47
48 15
49 16 In this study, we developed oral core-shell nanoparticles composed of curcumin
50
51
52 17 nanocrystals in the core and chitosan/alginate multilayers in the shell ¹² for inflammation-
53
54 18 targeted alleviation of ulcerative colitis (UC). Release rate of curcumin from the core-shell

1
2
3 19 nanoparticles was low at a pH mimicking the stomach and small intestine, whereas it was
4
5 20 higher at a pH mimicking the colon. Further, bio-distribution studies in the gastrointestinal
6
7 21 tract of mice showed that distribution of nanoparticles was significantly higher in colon
8
9 22 than that in stomach and small intestine. Quantitative analysis of drug in colonic tissues
10
11 23 and confocal imaging of colons revealed preferential accumulation of nanoparticles in
12
13 24 inflamed tissues than that in healthy tissues. *In vivo* anti-inflammatory studies revealed
14
15 25 that nanoparticles exhibit enhanced efficacy in alleviating inflammation-related symptoms
16
17 26 in mouse colitis model. The results suggest that the core-shell nanoparticles presented
18
19 27 here can be exploited as efficient colon-targeted drug delivery systems for UC therapy.
20
21
22
23
24

25
26 29 **KEYWORDS:** Chitosan, core-shell nanoparticles, curcumin nanocrystals, inflammation-targeted
27
28 30 delivery, sodium alginate, ulcerative colitis
29
30

31 31

32 32 **INTRODUCTION**

33 33
34 34
35 35
36 36
37 37

38 34 Ulcerative colitis (UC) is a chronic, recurrent inflammatory disease of the innermost lining of
39
40 35 the colon and rectum.^{1, 2} Delivery of orally administered drugs to the colon is highly desirable in
41
42 36 UC therapy, as it can result in low systemic toxicity and high efficacy of the drug.^{3, 4} However,
43
44 37 ¹² delivery of the ⁴ drugs to the colon is challenging owing to the physiological and anatomical barriers
45
46 38 associated with the gastrointestinal tract (GIT), such as degradation of the drug in acidic pH
47
48 39 conditions prevalent in the lumen, presence of digestive enzymes, and physical adsorption by the
49
50 40 mucosa.^{5, 6} To address these issues, various types of nanocarrier-based drug delivery systems, such
51
52 41 as polymeric nanoparticles,^{7, 8} lipid nanoparticles,⁹ silica nanoparticles,¹⁰ liposomes,^{11, 12}
53
54
55
56
57
58
59
60

1
2
3
4 42 nanoparticles in microparticles,¹³ and nanogels¹⁴ have been developed. However, low drug loading
5
6 43 capacity and excipient-associated side effects are intrinsic limitations associated with these drug
7
8 44 delivery systems. In addition, the fabrication cost of these systems is high.¹⁵⁻¹⁷ Therefore, to
9
10 45 overcome these limitations, new types of nanocarrier-based drug delivery systems are urgently
11
12 46 needed.

14 47 One promising approach to address these limitations is to fabricate drugs in nanocrystal
15
16 48 forms.^{18, 19} Unlike the other types of nanocarrier-based systems, the core of the drug nanocrystals
17
18 49 is entirely composed of the drug (~100 %) and stabilized using lesser amounts of excipient.²⁰⁻²² In
19
20 50 addition, the excipient-associated side effects can be minimized *in vivo* by using nanocrystals as
21
22 51 drug delivery systems. Thus, there is a substantial interest in the targeted delivery of the drug
23
24 52 nanocrystals to the colon. This will result in high doses of the drug molecule at the site of disease,
25
26 53 thus enhancing the therapeutic efficacy of the drugs. However, none of the fabricated drug
27
28 54 nanocrystals have been used till date for colon-targeted delivery to treat diseases such as UC. One
29
30 55 of the reasons for this is that the drug nanocrystals rapidly dissolve in the upper GIT following
31
32 56 oral administration before reaching the targeted colonic regions due to their small particle size.²⁰
33
34 57 In addition, the drug nanocrystals are reported to exhibit poor adhesion and accumulation in cells
35
36 58 and tissues.²³ Designing in-core-shell nanoparticles is one of the many strategies being investigated
37
38 59 for lowering the rate of drug dissolution from nanoparticles.²⁴ Core-shell nanoparticles are a class
39
40 60 of nanostructured materials comprising an inner core structure surrounded by external shells
41
42 61 prepared from different polymeric materials.²⁵ This unique structure has generated special interest
43
44 62 in using core-shell nanoparticles as carriers in the field of drug delivery. The key features of core-
45
46 63 shell nanoparticles include high drug loading efficiency and controlled drug release.^{24, 26}
47
48
49
50
51
52
53
54
55
56
57
58
59
60

1
2
3
4 64 In this study, we have developed curcumin nanocrystals (CUNCs) surrounded by chitosan
5
6 65 (CH), sodium alginate (AG), and cellulose acetate phthalate (CAP) polyelectrolyte multilayer
7
8 66 core-shell nanoparticles for colon-targeted therapy of UC. With this system, our goal is to deliver
9
10 67 CUNCs to the colon and ensuring that they are not dissolved in the upper GIT, thereby resulting
11
12 68 in a high availability of the drug in the colon for therapeutic activity. Further, we aimed at
13
14 69 enhancing the accumulation of CUNCs into inflamed colonic tissues by exploiting the surface-
15
16 70 charge reversing property of the multilayers surrounding the nanoparticles. In this study, the shell
17
18 71 of the core-shell nanoparticles was prepared using polyelectrolytes capable of changing the surface
19
20 72 charge of the shell from negative in the upper GIT to positive in the colon depending on pH
21
22 73 variation. In our earlier study, we had demonstrated that a pH-triggered surface charge-reversal of
23
24 74 nanoparticles promoted their adhesion and accumulation in the inflamed colonic tissues by
25
26 75 enabling their interaction with negatively charged-mucins in the mucosa during UC therapy.⁹
27
28
29
30
31
32

33 77 **MATERIALS AND METHODS**

34
35
36
37

38 79 **Materials**

39
40
41

42 81 Curcumin was purchased from Sigma-Aldrich (St. Louis, MO, USA). CH (Mw 50,000 -
43
44 82 190,000 Da, viscosity 20 - 30 cP and deacetylation ≥ 75 %), AG (Mw 80,000 - 120,000 Da,
45
46 83 viscosity ≥ 2000 cP and mannuronate/guluronate ratio 1.56), and CAP (Mw 2534.12, hydroxyl
47
48 84 content 3.6 % and acetyl content 39.8 %) were obtained from Sigma-Aldrich (St. Louis, MO,
49
50 85 USA). Dextran sodium sulfate (DSS) ¹ was obtained from MP Biomedicals (Irvine, CA, USA).
51
52 86 Mouse interleukin-6 (IL-6) DuoSet[®] ELISA KIT was purchased from R&D System (Minneapolis,
53
54
55
56
57
58
59
60

1
2
3 87 MN, USA). Tumor necrosis factor- α (TNF- α) ELISA MAX[®] was purchased from BioLegend Inc
4
5 88 (San Diego, CA, USA). Anti-rabbit IgG labeled with Alexa Flour 568 was purchased from Thermo
6
7 89 Fisher Scientific (Waltham, USA). Anti-F4/80 antibody and polyclonal anti-myeloperoxidase
8
9 90 were obtained from Abcam (Cambridge, UK). Alexa Flour 488-conjugated goat anti-mouse IgG
10
11 91 antibody was purchased from Jackson ImmunoResearch Inc (West Grove, PA, USA). All other
12
13 92 reagents and solvents were of the highest analytical grade commercially available.
14
15
16
17
18

19 94 **Preparation of core-shell nanoparticles**

20
21
22 95
23
24 96 CUNCs/CH, AG and CAP multilayer core-shell nanoparticles (CAP₁AG₄CH₅@CUNCs) were
25
26 97 prepared by ultrasound-assisted antisolvent crystallization and layer by layer (LBL)-coating
27
28 98 techniques (Figure 1A).^{27, 28} Briefly, curcumin (2 mg/mL in 60 % ethanol) was added to CH (2
29
30 99 mg/mL in 0.1 M acetic acid, pH 5) and sonicated (150 W/cm²) at 4°C for 30 min. The resulting
31
32 100 suspension was centrifuged at 20,000 × g for 20 min and washed thrice with 0.05 % NaCl to obtain
33
34 101 chitosan-coated curcumin nanocrystals (CH₁@CUNCs). CH₁@CUNCs were then re-suspended in
35
36 102 20 mL of AG solution (2 mg/mL in water, pH 5) and gently shaken for 20 min to allow AG coating
37
38 103 on the surfaces. The resulting suspension was centrifuged at 20,000 × g for 20 min and washed
39
40 104 thrice with 0.05 % NaCl. The coating was then continued using CH and AG alternately until the
41
42 105 desired number of CH/AG multilayer was obtained (AG₄CH₅@CUNCs). Finally,
43
44 106 AG₄CH₅@CUNCs were incubated in CAP solution (2 mg/mL, pH 6) for 20 min and washed thrice
45
46 107 with 0.05 % NaCl to obtain CAP₁AG₄CH₅@CUNCs.
47
48
49
50
51
52
53
54
55

54 109 **Characterization of core-shell nanoparticles**

1
2
3 110

4
5 111 The particle shape of CAP₁AG₄CH₅@CUNCs was characterized by scanning electron
6 112 microscopy (SEM) (SUPRA 40 VP ZEISS Ltd, USA). A drop of diluted suspension of
7
8
9 113 nanoparticles was placed ¹³ on a carbon tape, air dried at room temperature (25 °C) in a desiccator
10
11
12 114 and imaged at an accelerating voltage of 15 kV after coating with gold-palladium alloy. The core-
13
14 115 shell structure of CAP₁AG₄CH₅@CUNCs was characterized by transmission electron microscope
15
16 116 (TEM) (H7600 Hitachi, Japan) in accordance with a previously described procedure.²⁹

17
18 117 Dynamic light scattering (DLS) was used for measuring the particle size, polydispersity index
19
20 118 (PDI) and zeta potential of CAP₁AG₄CH₅@CUNCs by ¹¹ Malvern Zetasizer Nano ZS90, (Malvern
21
22 119 Panalytical, UK). Three independent samples of nanoparticles were diluted in water, dispersed
23
24
25 120 well, and measured at a fixed angle of 137° at 25 °C.

26
27 121 Differential scanning calorimetry (DSC) was performed using PerkinElmer DSC instrument
28
29 122 (Waltham, USA) to examine the crystalline state of curcumin in CH₁@CUNCs and
30
31 123 CAP₁AG₄CH₅@CUNCs. Five milligrams of curcumin powder, CH₁@CUNCs and
32
33 124 CAP₁AG₄CH₅@CUNCs were accurately weighed and heated at a temperature ranging from 0 -
34
35 125 300 °C with a heating rate of 10 °C/min.

36
37
38
39
40 126

41 42 127 **pH-dependent drug release study**

43
44
45 128

46
47 129 To study the effect of pH on drug release rate, CAP₁AG₄CH₅@CUNCs ¹¹ were studied using a
48
49 130 gradually pH-changing buffer solution that mimicked the pH variation in the human GIT.³⁰ Briefly,
50
51 131 22.5 mg of nanoparticles was ¹⁵ suspended in 50 mL of 0.1 N hydrochloric acid (pH 1.2) and agitated
52
53 132 (60 rpm) at 37 °C for 2 ⁵ h. The pH of the buffer was then increased to 4.5 by adding a powder

1
2
3 133 mixture containing 2.28 g of tris(hydroxymethyl) aminomethane and 1.77 g of anhydrous sodium
4
5 134 acetate and the experiment was performed for 3 h. The pH of the buffer was further increased to
6
7
8 135 7.2 by adding the same powder mixture again and the study was continued till completion, i.e.,
9
10 136 24 h. At predetermined time intervals, 500 μL of the sample was collected from the solution
11
12 137 and centrifuged at $45,000 \times g$ at 4°C for 30 min. Then, the drug content in the supernatant
13
14 138 was analyzed by high-performance liquid chromatography (HPLC)³¹ and the pellet was
15
16 139 redispersed in the release buffer solution with 500 μL of fresh medium to avoid the loss
17
18 140 of nanoparticles. The HPLC system (Shimadzu, Tokyo, Japan) used was equipped with an
19
20 141 autosampler processor, SPD-20A ultraviolet (UV) detector, and C18 column ($5 \mu\text{m}$, $250 \text{ mm} \times 4.6$
21
22 142 mm). The mobile phase consisting of a mixture of methanol: H_2O (containing 3.6 % glacial acetic
23
24 143 acid) (73:27, v/v) was pumped at a flow rate of 1 mL/min. The sample injection volume was set at
25
26 144 $20 \mu\text{L}$ and the UV detector was set at 306 nm. The retention time was 7.5 min at 25°C .
27
28
29
30
31
32

33 146 pH-dependent charge-reversing study

34
35 147
36
37 148 The surface charge-reversing property of $\text{CAP}_1\text{AG}_4\text{CH}_5@\text{CUNCs}$ was studied by measuring
38
39 149 their zeta-potential at different pH values following previously described procedure.⁹ The
40
41 150 nanoparticles were added to the buffers with different pH values, similar to the varying pH
42
43 151 conditions in the human GIT (stomach 1.2, small intestine 4.5 and colon 7.2) and incubated in a
44
45 152 shaking water bath (60 rpm) at 37°C for predetermined times. Then, the nanoparticles were
46
47 153 collected by centrifugation at $20,000 \times g$ for 20 min and washed thrice with distilled water ($20,000$
48
49 $\times g$ for 20 min). Finally, they were re-suspended in distilled water and surface charge was measured
50
51 154 using DLS method (Malvern Zetasizer Nano ZS90, Malvern Panalytical, UK).
52
53
54
55
56
57
58
59
60

156

Bio-distribution of core-shell nanoparticles in mice GIT

158

159 The bio-distribution of CH₁@CUNCs and core-shell nanoparticles in the different segments
160 of the GIT in colitis-induced mice was studied. Briefly, mice were randomly divided into the
161 following four groups (*n* = 6 mice per group): control (no drug treatment), CH₁@CUNCs,
162 AG₄CH₅@CUNCs (core-shell nanoparticles without CAP layer), and CAP₁AG₄CH₅@CUNCs.
163 Nanoparticle suspensions were prepared and orally administered to mice (curcumin concentration
164 of 50 mg/kg of body weight) for 6 h or 12 h. At the end of each experiment, the mice were
165 euthanized and the GIT segments, including luminal contents were excised. The drug contents
166 from different segments, such as stomach, small intestine and colon were then analyzed using
167 HPLC.³²

168 The bio-distribution of CH₁@CUNCs and core-shell nanoparticles in mice GIT was also
169 studied using an *in vivo* imaging system (IVIS) (FOBS; Nanoscience, South Korea). For
170 fluorescent imaging of mice GIT, IR-780 dye was used as fluorescent probe after assembling with
171 curcumin in core-shell nanoparticles.³³ Briefly, mice were divided into 4 experimental groups (*n*
172 = 6 in each group). The control group did not receive any drug, while the other groups were orally
173 administered with CH₁@CUNCs, AG₅CH₅@CUNCs, or CAP₁AG₄CH₅@CUNCs at a curcumin
174 dose of 0.5 mg/kg. After 6 h or 12 h of administration, the mice were euthanized and the entire
175 GIT was excised for *ex vivo* fluorescence imaging.

176

Accumulation of core-shell nanoparticles into inflamed colonic tissues

178

1
2
3 179 The accumulation of CH₁@CUNCs and core-shell nanoparticles in the inflamed colonic tissues
4
5 of mice was analyzed quantitatively and the results were compared to that in healthy colons.⁹
6
7 8 Briefly, mice were divided into 4 groups (*n* = 6 in each group). The control group did not receive
8
9 8 drug, while the other groups were orally administered with CH₁@CUNCs, AG₅CH₅@CUNCs or
10
11 8 CAP₁AG₄CH₅@CUNCs at a curcumin dose of 50 µg per mice. After 12 h of administration, mice
12
13 8 were euthanized, colons were excised, and samples from healthy and inflamed colons were freeze-
14
15 184 dried. Thirty milligrams of healthy and inflamed colon samples were used to extract curcumin with
16
17 185 one milliliter of ethanol and the drug concentrations in the samples were quantified by HPLC.³⁴
18
19 186

20
21 12 To further investigate the accumulation of CH₁@CUNCs and core-shell nanoparticles in
22
23 12 inflamed colonic tissues of mice, confocal laser scanning microscopy (CLMS) (Olympus FV10i,
24
25 188 Tokyo, Japan) was used. For confocal imaging of the colonic tissues of mice, curcumin was used
26
27 189 as fluorescence probe.³⁰ Samples from inflamed colons were fixed in 4 % paraaldehyde prepared in
28
29 190 10 % sucrose for 12 h at 4 °C. The colon samples were then embedded in Tissue-Tek® O.C.T.
30
31 191 compound (Sakura, Netherlands), cut into 5 µm sections, and visualized.
32
33 192
34
35 193

37 194 **Animal model and treatments**

38
39 195
40
41 6 All animal studies in this work were in compliance with the regulations of Pusan National
42
43 6 University, Busan, South Korea (PNU-IACUC, approval number: PNU-2018-2038). Imprinting
44
45 14 control region (ICR) mice (30 - 35 g body weight) were housed at the university animal center at
46
47 14 25 ± 3 °C under a 12 h light/dark cycle for 7 days before the induction of colitis. Colitis was
48
49 199 induced in mice by supplementing 2.5 % (w/v) DSS in drinking water for 7 days. Age and sex-
50
51 200 matched mice were given access to tap water and considered as healthy control group. After the
52
53 1
54 201
55
56
57
58
59
60

1
2
3 202 ¹⁰ induction of colitis, DSS water was replaced with normal tap water and drug treatment was started.
4

5 203 Mice were divided into five experimental groups: healthy control, colitis control, CH₁@CUNCs-

6
7 204 treated, AG₅CH₅@CUNCs-treated and CAP₁AG₄CH₅@CUNCs-treated. ⁴ The mice in drug-treated

8
9 205 groups received an equal dose of a curcumin (15 mg/kg) in the form of suspension by oral gavage

10
11 206 for 7 days. Mice in healthy and colitis groups did not receive any curcumin.
12
13
14

15 207

16 208 **Macroscopic grading of colitis**

17
18
19 209

20
21
22 210 The macroscopic assessment of colitis was performed based on disease activity index (DAI),

23
24 211 colon length and spleen weight of mice. DAI was monitored blindly, starting from first day of

25
26 212 induction of colitis until the last day of treatment, and includes a sum of 3 parameters: ¹⁵ body weight,

27
28 213 stool consistency, and rectal bleeding.³⁵ Briefly, the loss in body weight was scored in a four point

29
30 214 scale: no weight loss was assigned a score of 0, 1 – 5 % weight loss was assigned a score of 1, 5 –

31
32 215 10 % of weight loss was assigned a score of 2, 10 - 20% weight loss was assigned a score of 3,

33
34 216 and > 20 % weight loss was assigned a score of 4. Similar scaling was used for stool consistency:

35
36 217 ⁷ well-formed pellets stool was assigned 0, semi-formed stool was assigned a score of 2, and liquid

37
38 218 stool was assigned a score of 4 points. Similarly, for rectal bleeding: no blood was assigned a score

39
40 219 of 0, positive finding was assigned a score of 2, and gross bleeding was assigned a score of 4. ⁷ All

41
42 220 mice were euthanized by CO₂ asphyxiation after 24 h of last drug treatment and the colon and

43
44 221 spleen were carefully removed. Resected colon and spleen were rinsed with cold phosphate buffer

45
46 222 and colon length and spleen weight were measured as gross clinical features for assessing the

47
48 223 colitis severity.³⁶

49
50 224
51
52
53
54
55
56
57
58
59
60

225 **Histological analysis of colitis**

226

227 To evaluate the therapeutic efficacy of core-shell nanoparticles on the severity of colitis,
228 histological analysis of mice colon tissues was performed using Hematoxylin-Eosin (H&E)
229 staining. The mice colon samples were fixed in neutral buffer with 10 % formalin and embedded
230 in wax. The embedded colons were then cut into 5 μm -thick sections using microtome (Reichert,
231 Munich, Germany), stained with H&E, and scanned using light microscopy (Zeiss, Axioskop,
232 Germany). The severity of colitis in each colonic section was assessed by evaluating mucosal
233 features, such as epithelium damage, mucosal edema, and infiltration of inflammatory cells into
234 mucosa using a blinded approach.³⁷

235

236 **Neutrophil and macrophage infiltration into mucosa**

237

238 Immunofluorescence was performed on the colon samples for detecting neutrophil and
239 macrophage infiltration in mucosa.³⁸ Formalin-fixed paraffin-embedded colon samples were cut
240 into 5 μm -thick sections using microtome (Reichert, Munich, Germany) and incubated with
241 blocking solution (Tris buffer with 2 % BSA). Further, to detect neutrophil infiltration, the tissue
242 sections were incubated overnight with polyclonal anti-myeloperoxidase (1:200 dilution) at 4 °C,
243 followed by incubation with the secondary antibody Alexa Flour 488-conjugated goat anti-mouse
244 IgG (1:200 dilution) for 1 h at 25 °C. Similarly, for detecting macrophage infiltration, the tissue
245 sections were incubated overnight with primary anti-F4/80 antibody (1:500 dilution) at 4°C,
246 followed by incubation with anti-rabbit IgG labeled with Alexa Flour 568 (1:200 dilution)
247 secondary antibody for 3 h at 25°C. Finally, the colonic sections were counterstained with 5 $\mu\text{g}/\text{mL}$

1
2
3 of 4',6-diamidino-2-phenylindole (DAPI) and analyzed using confocal microscopy (Olympus
4
5
6 FV10i, Tokyo, Japan).

7
8 250

9
10 251 **Measurement of MPO activity and pro-inflammatory cytokine levels**

11
12 252

13
14
15 253 MPO activity in the colon tissues was measured by following a previously described method.³⁹

16
17 254 Briefly, 50 mg of the tissue sample was homogenized in 2 mL of ice-cold 50 mM phosphate buffer

18
19 255 (pH 6.0) containing 0.5% hexa-decyltrimethyl ammonium bromide at 30 Hz and 4 °C for 4 min.

20
21 256 The homogenate was then centrifuged at 13,400 × g for 6 min at 4°C. The supernatant was then

22
23 257 collected and added to 0.0167% o-dianisidine hydrochloride (o-dianisidine) solution and 0.0005%

24
25 258 hydrogen peroxide (H₂O₂), and the change in absorbance was measured at 450 nm at intervals of

26
27 259 30 s. The o-dianisidine solution was prepared by dissolving 16.7 mg of o-dianisidine in 90 mL of

28
29 260 distilled water and 10 mL of 50 mM phosphate buffer. MPO activity was calculated as a unit of

30
31 261 MPO per mg of tissue. One unit of MPO was defined as the amount needed to degrade 1 μmol

32
33 262 H₂O₂ per min.

34
35 263 The concentration of interleukin-6 (IL-6) and tumor necrosis factor (TNF-α) were quantified

36
37 264 in the colons samples according to an established method described by Kim et al.³⁹ Briefly, 50 mg

38
39 265 of the colon tissue samples were homogenized in 1 mL of protease inhibitor cocktail and lysis

40
41 266 buffer solution (10 mL of 1 M tris-hydrochloric acid (pH = 8.0), 6 mL of 5 M sodium chloride and

42
43 267 2 mL of Triton X-100 in 182 mL of sterilized distilled water) for 5 min at 30 Hz. The homogenate

44
45 268 was centrifuged at 3300 × g for 5 min at 4 °C and the supernatant was used to quantify IL-6 and

46
47 269 TNF-α by a sandwich-type enzyme-linked immunosorbent assay as per the supplier's instructions.

48
49 270

1
2
3 **271 RESULTS**
4

5
6 **272**

7
8 **273 Preparation and characterization of core-shell nanoparticles**
9

10 **274**

11
12 In this study, CH₁@CUNCs were prepared using the anti-solvent crystallization technique
13 (Figure 1A). The curcumin solution was added to the CH solution to form CH₁@CUNCs under
14 (Figure 1A). The curcumin solution was added to the CH solution to form CH₁@CUNCs under
15 (Figure 1A). The curcumin solution was added to the CH solution to form CH₁@CUNCs under
16 (Figure 1A). The curcumin solution was added to the CH solution to form CH₁@CUNCs under
17 (Figure 1A). The curcumin solution was added to the CH solution to form CH₁@CUNCs under
18 (Figure 1A). The curcumin solution was added to the CH solution to form CH₁@CUNCs under
19 (Figure 1A). The curcumin solution was added to the CH solution to form CH₁@CUNCs under
20 (Figure 1A). The curcumin solution was added to the CH solution to form CH₁@CUNCs under
21 (Figure 1A). The curcumin solution was added to the CH solution to form CH₁@CUNCs under
22 (Figure 1A). The curcumin solution was added to the CH solution to form CH₁@CUNCs under
23 (Figure 1A). The curcumin solution was added to the CH solution to form CH₁@CUNCs under
24 (Figure 1A). The curcumin solution was added to the CH solution to form CH₁@CUNCs under
25 (Figure 1A). The curcumin solution was added to the CH solution to form CH₁@CUNCs under
26 (Figure 1A). The curcumin solution was added to the CH solution to form CH₁@CUNCs under
27 (Figure 1A). The curcumin solution was added to the CH solution to form CH₁@CUNCs under
28 (Figure 1A). The curcumin solution was added to the CH solution to form CH₁@CUNCs under
29 (Figure 1A). The curcumin solution was added to the CH solution to form CH₁@CUNCs under
30 (Figure 1A). The curcumin solution was added to the CH solution to form CH₁@CUNCs under
31 (Figure 1A). The curcumin solution was added to the CH solution to form CH₁@CUNCs under
32 (Figure 1A). The curcumin solution was added to the CH solution to form CH₁@CUNCs under
33 (Figure 1A). The curcumin solution was added to the CH solution to form CH₁@CUNCs under
34 (Figure 1A). The curcumin solution was added to the CH solution to form CH₁@CUNCs under
35 (Figure 1A). The curcumin solution was added to the CH solution to form CH₁@CUNCs under
36 (Figure 1A). The curcumin solution was added to the CH solution to form CH₁@CUNCs under
37 (Figure 1A). The curcumin solution was added to the CH solution to form CH₁@CUNCs under
38 (Figure 1A). The curcumin solution was added to the CH solution to form CH₁@CUNCs under
39 (Figure 1A). The curcumin solution was added to the CH solution to form CH₁@CUNCs under
40 (Figure 1A). The curcumin solution was added to the CH solution to form CH₁@CUNCs under
41 (Figure 1A). The curcumin solution was added to the CH solution to form CH₁@CUNCs under
42 (Figure 1A). The curcumin solution was added to the CH solution to form CH₁@CUNCs under
43 (Figure 1A). The curcumin solution was added to the CH solution to form CH₁@CUNCs under
44 (Figure 1A). The curcumin solution was added to the CH solution to form CH₁@CUNCs under
45 (Figure 1A). The curcumin solution was added to the CH solution to form CH₁@CUNCs under
46 (Figure 1A). The curcumin solution was added to the CH solution to form CH₁@CUNCs under
47 (Figure 1A). The curcumin solution was added to the CH solution to form CH₁@CUNCs under
48 (Figure 1A). The curcumin solution was added to the CH solution to form CH₁@CUNCs under
49 (Figure 1A). The curcumin solution was added to the CH solution to form CH₁@CUNCs under
50 (Figure 1A). The curcumin solution was added to the CH solution to form CH₁@CUNCs under
51 (Figure 1A). The curcumin solution was added to the CH solution to form CH₁@CUNCs under
52 (Figure 1A). The curcumin solution was added to the CH solution to form CH₁@CUNCs under
53 (Figure 1A). The curcumin solution was added to the CH solution to form CH₁@CUNCs under
54 (Figure 1A). The curcumin solution was added to the CH solution to form CH₁@CUNCs under
55 (Figure 1A). The curcumin solution was added to the CH solution to form CH₁@CUNCs under
56 (Figure 1A). The curcumin solution was added to the CH solution to form CH₁@CUNCs under
57 (Figure 1A). The curcumin solution was added to the CH solution to form CH₁@CUNCs under
58 (Figure 1A). The curcumin solution was added to the CH solution to form CH₁@CUNCs under
59 (Figure 1A). The curcumin solution was added to the CH solution to form CH₁@CUNCs under
60 (Figure 1A). The curcumin solution was added to the CH solution to form CH₁@CUNCs under
prepared (Table 1).

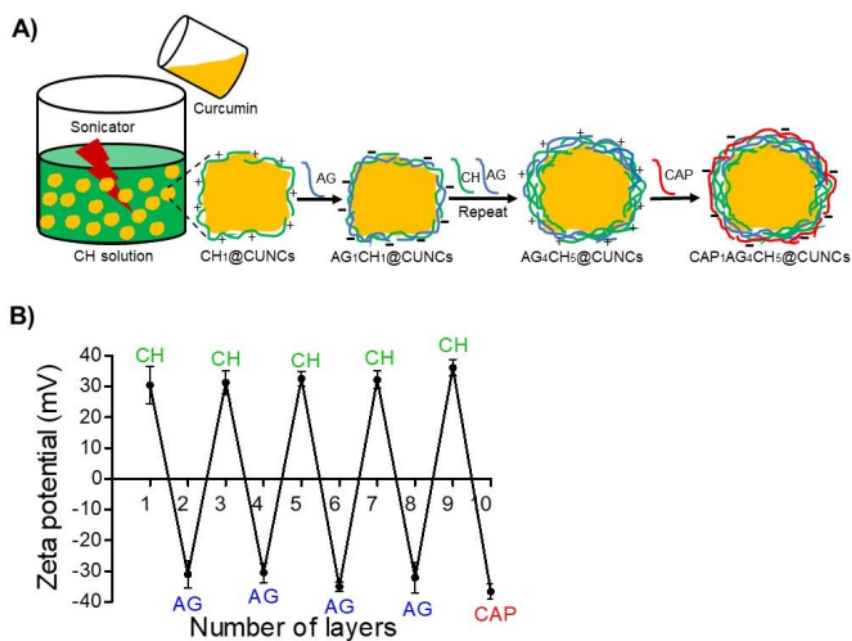
31
32 **281**
33 **282 Table 1.** Physicochemical characteristics of core-shell nanoparticles
34

1 Formulation	Particle size (nm)	PDI	Zeta potential (mV)	Drug loading (%)
CH ₁ @CUNCs	380 ± 90	0.09 ± 0.02	+ 34 ± 7	94 ± 7
AG ₅ CH ₅ @CUNCs	420 ± 17	0.29 ± 0.04	- 36 ± 2	90 ± 4
CAP ₁ AG ₄ CH ₅ @CUNCs	421 ± 14	0.21 ± 0.01	- 47 ± 3	91 ± 3

41 **13**
42 **283** Note: results are expressed as mean ± SD (*n* = 3).
43
44 **284**

45
46 **285** To prepare CAP₁AG₄CH₅@CUNCs, CH₁@CUNCs were coated with multiple layers of CH
47 and AG followed by CAP using an LBL-coating technique. To confirm the coating of CH, AG,
48 and CAP on CH₁@CUNCs surface, zeta potential of the resulted particles was measured during
49 every coating step. Successful coating of each polyelectrolyte layer was confirmed based on the
50 change in charge between positive and negative during every coating step, as shown in Figure 1B.
51
52
53
54
55
56
57
58
59
60

1
2
3 290 Analysis of $\text{CH}_1@\text{CUNCs}$ and $\text{CAP}_1\text{AG}_4\text{CH}_5@\text{CUNCs}$ using SEM confirmed the cubic shape of
4
5 291 nanoparticles (Figure 2A and C). Moreover, TEM was used to analyze the core-shell structure of
6
7 292 $\text{CH}_1@\text{CUNCs}$ and $\text{CAP}_1\text{AG}_4\text{CH}_5@\text{CUNCs}$ (Figure 2B and D, respectively). As shown in Figure
8
9
10 293 2D, the high contrast dark black region indicates the CUNCs core, whereas, the light darker part
11
12 294 surrounding the core confirms the presence of CH/AG/CAP multilayer shell. The diameter of the
13
14 295 curcumin core was approximately 270 - 280 nm, while the thickness of the CH/AG/CAP multilayer
15
16 296 shells was approximately 50 - 100 nm (Figure 2D). In general, it has been reported that the core-
17
18 297 shell nanoparticles with thick shell have the advantage of achieving a sustained drug release from
19
20 298 their inner cores.⁴¹
21
22
23
24 299



300

301

302 **Figure 1.** Preparation of core-shell nanoparticles and their zeta potential at different stages. (A)

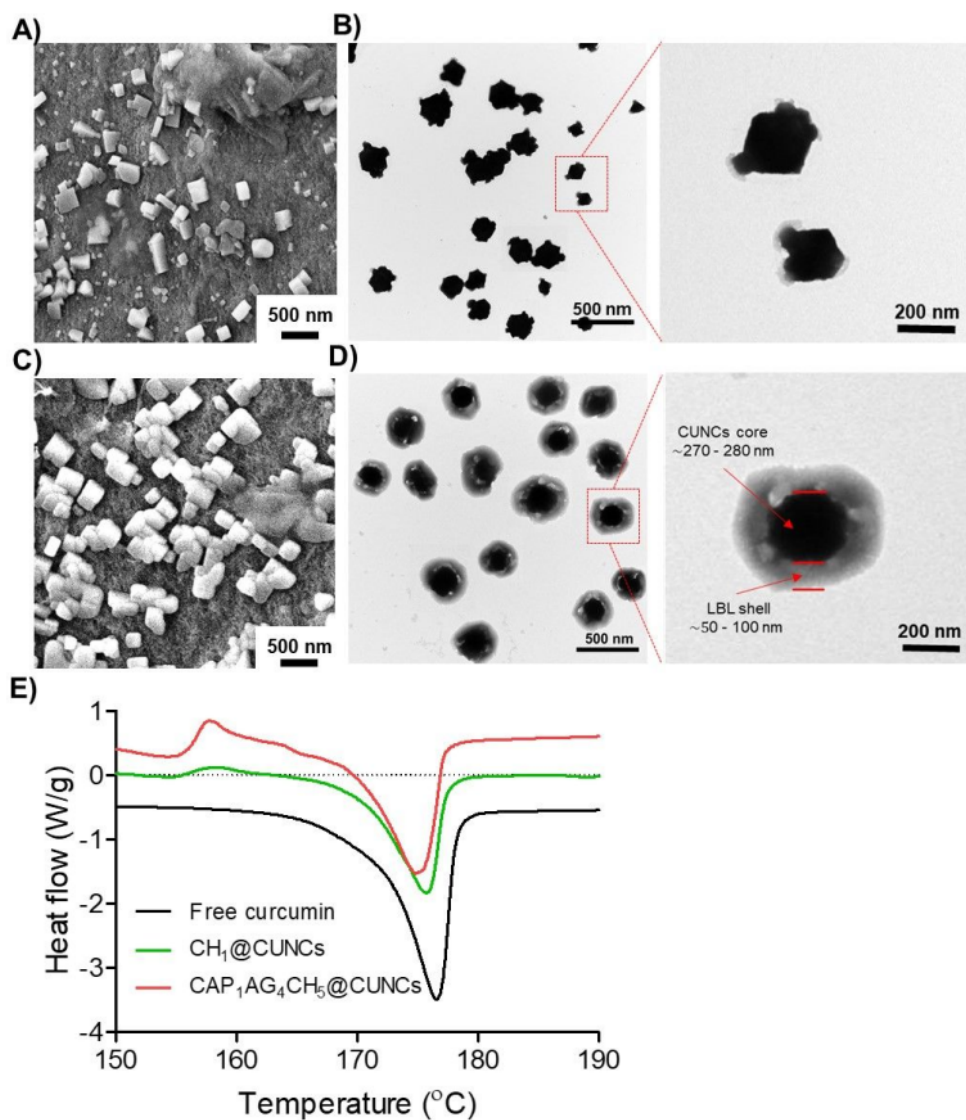
303 Schematic diagram of $\text{CAP}_1\text{AG}_4\text{CH}_5@\text{CUNCs}$ preparation using ultrasound-assisted antisolvent

58
59
60

1
2
3 304 crystallization and LBL-coating techniques. (B) Change in zeta-potential of CH₁@CUNCs as a
4
5 305 function of the number of CH, AG, and CAP layers during the preparation of
6
7 306 CAP₁AG₄CH₅@CUNCs. Data are represented as means ± SD (*n* = 6).
8
9

10 307
11
12 308 CAP₁AG₄CH₅@CUNCs with an average diameter of 421 ± 14 nm and PDI of 0.21 ± 0.01 were
13
14 309 successfully prepared in this study (Table 1). The small PDI value indicated the narrow particle
15
16 310 size distribution of CAP₁AG₄CH₅@CUNCs. To examine the crystalline state of curcumin in the
17
18 311 core, DSC analysis was performed for CH₁@CUNCs and CAP₁AG₄CH₅@CUNCs and was
19
20 312 compared with that of curcumin powder. CAP₁AG₄CH₅@CUNCs showed endotherm peaks with
21
22 313 a melting point at ~ 175 °C, which coincided with that of free curcumin and CH₁@CUNCs (Figure
23
24 314 2E), indicating that the crystalline state of CH₁@CUNCs was not affected by the LBL-coating
25
26 315 process.
27
28
29

30 316 CAP₁AG₄CH₅@CUNCs showed a high drug loading efficiency with up to 90 % for curcumin.
31
32 317 Although, the drug loading efficiency of CAP₁AG₄CH₅@CUNCs was found to be slightly lesser
33
34 318 than that of CH₁@CUNCs, it was insignificant (Table 1). Further, it should be noted that ¹high drug
35
36 319 content is one of the important advantages of drug delivery systems prepared by the LBL-coating
37
38 320 technique.⁴²
39
40
41
42
43
44
45
46
47
48
49
50
51
52
53
54
55
56
57
58
59
60



321

322 **Figure 2.** Physical characterization of core-shell nanoparticles. SEM and TEM images of
323 $\text{CH}_1@CUNCs$ (A and B, respectively) and $\text{CAP}_1\text{AG}_4\text{CH}_5@CUNCs$ (C and D, respectively),
324 indicating the core-shell structure of nanoparticle. (E) DSC peak of free curcumin, $\text{CH}_1@CUNCs$
325 and $\text{CAP}_1\text{AG}_4\text{CH}_5@CUNCs$.

326

327 pH-dependent drug release and charge-reversal studies

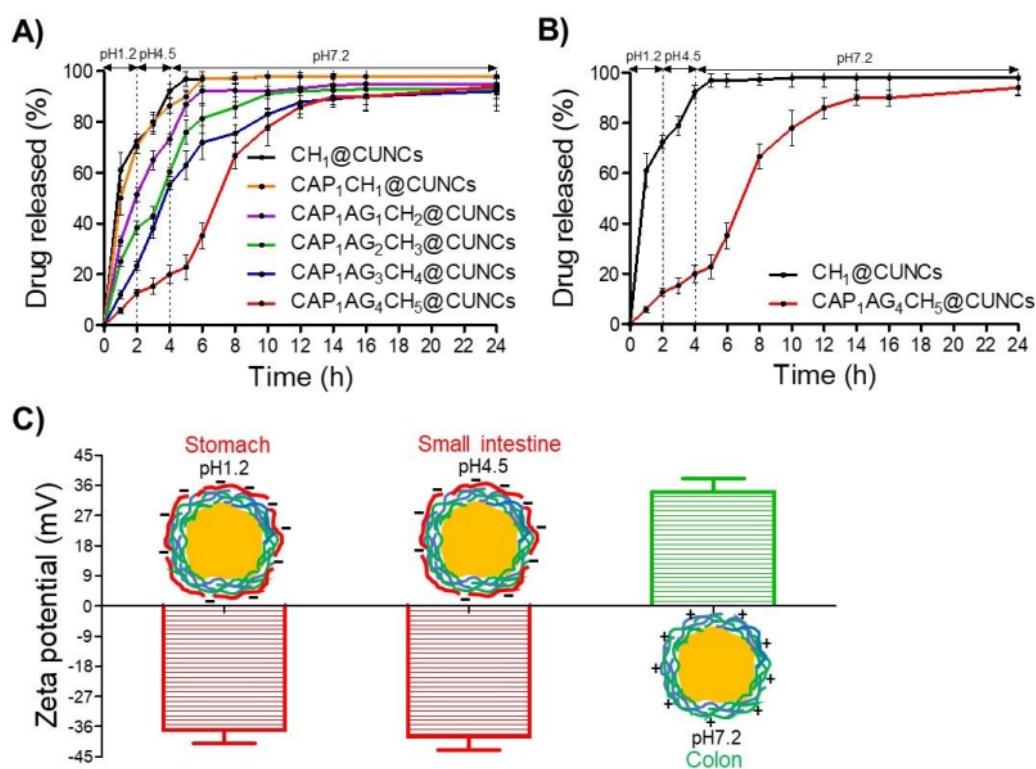
328

329 To evaluate the effect of shell thickness on pH-dependent drug release, core-shell nanoparticles
330 with different shell thickness (different number of CH/AG/CAP multilayers) were prepared (Table
331 1 and Table S1). Drug release from core-shell nanoparticles was shown to be reduced in the first
332 5 h at pH 1.2 and 4.5 by increasing the number of CH/AG/CAP multilayers. Approximately, 20 -
333 80 % of total curcumin was released from core-shell nanoparticles depending on the number of
334 CH/AG/CAP multilayers (Figure 3A). However, core-shell nanoparticles with less than 10
335 multilayers of CH/AG/CAP, such as CAP₁AG₁CH₂@CUNCs, CAP₁AG₂CH₃@CUNCs, and
336 CAP₁AG₃CH₄@CUNCs showed burst drug release at pH 1.2 and 4.5. Further, core-shell
337 nanoparticles with 10 CH/AG/CAP multilayers, CAP₁AG₄CH₅@CUNCs, showed ~3-fold lesser
338 curcumin release than others at pH 1.2 and 4.5. Total curcumin released from
339 CAP₁AG₄CH₅@CUNCs at pH 1.2 and 4.5 was ~20 % (Figure 3B). However, by increasing the
340 pH of the buffer to 7.2, CAP₁AG₄CH₅@CUNCs showed sustained drug release with the remaining
341 curcumin payload released in ~9 h (Figure 3A). These results indicate that the shell thickness of
342 50 - 100 nm having 10 CH/AG/CAP layers (CAP₁AG₄CH₅@CUNCs) is responsible for the
343 controlled drug release from the nanoparticle cores. This hypothesis was partially supported by the
344 release profile of AG₅CH₅@CUNCs, which exhibited burst drug release at pH 1.2 and 4.5.
345 Approximately 80 % of the total drug payload of AG₅CH₅@CUNCs was released in the first 5 h
346 of the study at pH 1.2 and 4.5 (Figure 3B).

347 The pH-dependent charge reversal property of the core-shell nanoparticles was studied by
348 measuring their zeta-potential in buffer solutions with different pH (Figure 3C).
349 CAP₁AG₄CH₅@CUNCs exhibited negative surface charge of -37 ± 4 mV and -36 ± 5 mV at pH

1
2
3 350 1.2 and 4.5, respectively, owing to the presence of CAP outer layer. In contrast, in a buffer with
4
5 351 pH 7.2, CAP₁AG₄CH₅@CUNCs exhibited a positive surface charge of 34 ± 4 mV, because of the
6
7 352 dissolution of CAP outer layer and exposure of the CH layer beneath.
8
9

10 353



354

355 **Figure 3.** Drug release and charge reversal properties of the nanoparticles based on pH variation.

356 (A) pH-dependent drug release from core-shell nanoparticles with shells containing different

357 numbers of CH/AG/CAP multilayers. (B) pH-dependent drug release from AG₅CH₅@CUNCs and

358 CAP₁AG₄CH₅@CUNCs. (C) pH-dependent surface charge reversal of CAP₁AG₄CH₅@CUNCs.

359 Data are represented as means \pm SD ($n = 6$).

360

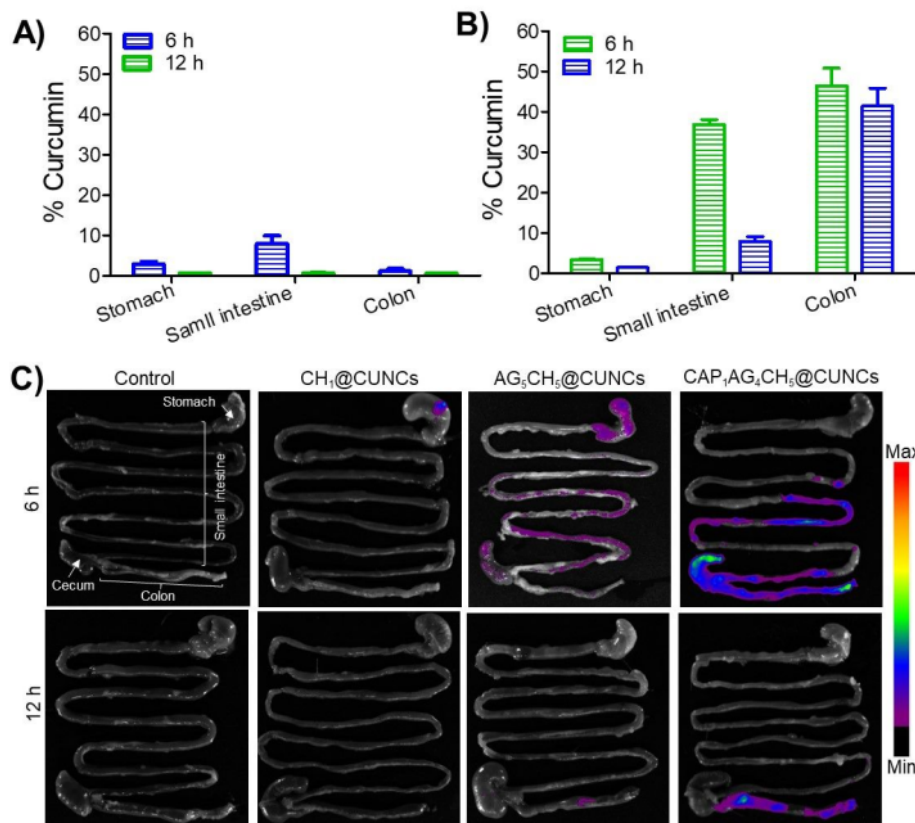
361 **Bio-distribution of core-shell nanoparticles in mice GIT**

362

363 Figure 4A and B show the maximum recovery of curcumin from the different GI tract
364 segments after 6 and 12 h post-administration of CH₁@CUNCs and core-shell nanoparticles to
365 mice. For AG₅CH₅@CUNCs, ~ 8 % of curcumin was recovered from the small intestine after 6 h
366 post-administration, whereas trace amounts of curcumin were detected in stomach as well as colon
367 (Figure 4A). After 12 h post-administration of AG₅CH₅@CUNCs, negligible amounts of curcumin
368 were detected in the stomach, small intestine and colon. The reason for the small amounts of
369 curcumin recovered after 6 h and 12 h post-administration of AG₅CH₅@ CUNCs is presumably
370 due to the systemic absorption of curcumin in the stomach and small intestine before reaching the
371 colon. For CAP₁AG₄CH₅@CUNCs, maximum recovery of ~ 45 % and ~ 40 % of curcumin was
372 achieved from the colon after 6 and 12 h post-administration, respectively (Figure 4B). The drug
373 recovery from CAP₁AG₄CH₅@CUNCs in case of the small intestine was found to be ~ 35 % and
374 ~ 7 % 6 and 12 h post-administration to mice, respectively, and negligible amounts were found in
375 the stomach (Figure 4B). It was worth to mention that no curcumin was recovered from the
376 stomach, small intestine and colon after 6 and 12 h post-administration of CH₁@CUNCs to mice.

377 Figure 4C shows representative IVIS images demonstrating the bio-distribution of
378 CH₁@CUNCs and core-shell nanoparticles in different GIT segments after 6 and 12 h post-
379 administration. CH₁@CUNCs showed no significant fluorescent signal in the GIT segments after
380 6 and 12 h post-administration to mice. For AG₅CH₅@CUNCs, weak fluorescence signals were
381 detected in the stomach, small intestine, and cecum (not colon) after 6 h post-administration, which
382 completely disappeared after 12 h (Figure 4C). These results proved that AG₅CH₅@CUNCs had
383 dissolved in the stomach and small intestine before reaching the colon. In contrast,

1
2
3 384 CAP₁AG₄CH₅@CUNCs showed high fluorescence signals in the small intestine and colon after 6
4
5 385 h, with signals being detected in the colon after 12 h post-administration (Figure 4C). These results
6
7 386 indicated that CAP₁AG₄CH₅@CUNCs are more efficiently distributed in the colon as compared
8
9 387 to CH₁@CUNCs and AG₅CH₅@CUNCs.
10
11
12 388
13
14 389
15
16
17



390

391

392 **Figure 4.** Bio-distribution of CH₁@CUNCs and core-shell nanoparticles in different segments of
393 mice GIT. Quantitative analysis indicating bio-distribution of AG₅CH₅@CUNCs (A) and
394 CAP₁AG₄CH₅@CUNCs (B) in different mice GIT segments 6 and 12 h post- administration. (C)

395

396

397

398

399

400

401

402

403

404

405

1
2
3 395 IVIS images of mice GIT showing the bio-distribution of CH₁@CUNCs, AG₅CH₅@CUNCs and
4
5 396 CAP₁AG₄CH₅@CUNCs 6 and 12 h post-administration to mice. Data are represented as means ±
6
7
8 397 SD (*n* = 6).
9

398

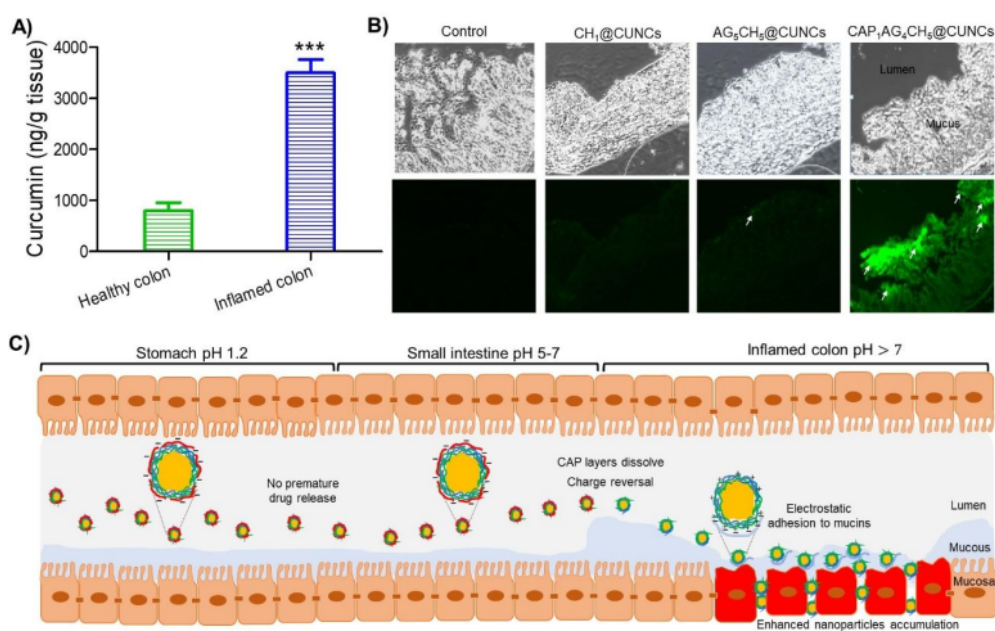
399 **Accumulation of core-shell nanoparticles in the inflamed colonic tissues**

400

17 401 The accumulation of CH₁@CUNCs and core-shell nanoparticles in the inflamed colons was
18
19 402 analyzed quantitatively and compared to that of healthy colons (Figure 5A). For mice administered
20
21 403 with CAP₁AG₄CH₅@CUNCs, significant amounts of curcumin were recovered from the healthy
22
23 404 and inflamed colonic tissues. However, the concentration of the curcumin recovered from the
24
25 405 inflamed tissues (3500 ng/g tissue) was significantly higher (*p* < 0.001) than that from healthy
26
27 406 colon (798 ng/g tissue) (Figure 5A). These results indicate that CAP₁AG₄CH₅@CUNCs
28
29 407 accumulate more effectively in the inflamed colonic tissues than in healthy colonic tissues,
30
31 408 presumably *via* the charge-reversal properties of core-shell nanoparticles. As expected, no
32
33 409 curcumin was recovered from both healthy and inflamed colonic tissues obtained from mice
34
35 410 administered with CH₁@CUNCs or AG₅CH₅@CUNCs.
36
37

39 411 We further investigated the accumulation of CH₁@CUNCs and core-shell nanoparticles in the
40
41 412 inflamed colonic tissues of colitis using a confocal microscopy. Figure 5B shows confocal images
42
43 413 of colons demonstrating the accumulation of CH₁@CUNCs and core-shell nanoparticles in the
44
45 414 inflamed colonic tissues of colitis mice. No fluorescence signal was detected in the colonic tissue
46
47 415 of mice with CH₁@CUNCs, indicating that few nanoparticles are accumulated in the colonic
48
49 416 tissues. For mice with AG₅CH₅@CUNCs, the signal was too weak to distinguish it from the
50
51 417 colonic tissue autofluorescence (Figure 5B). In contrast, the inflamed colonic tissues of the
52
53
54
55
56
57
58
59
60

1
2
3
4 418 mice administered with $\text{CAP}_1\text{AG}_4\text{CH}_5@\text{CUNCs}$ showed stronger fluorescence signals than
5
6 419 those treated with $\text{CH}_1@\text{CUNCs}$ or $\text{AG}_5\text{CH}_5@\text{CUNCs}$. At 12 h post-administration of mice,
7
8 420 $\text{CAP}_1\text{AG}_4\text{CH}_5@\text{CUNCs}$ highly accumulated in the inflamed colonic tissues (Figure 5B).
9
10 421 These results were consistent with the curcumin quantitative results and further indicated that
11
12 422 $\text{CAP}_1\text{AG}_4\text{CH}_5@\text{CUNCs}$ were more preferentially accumulated in the inflamed colonic tissues of
13
14 423 mice than $\text{CH}_1@\text{CUNCs}$ and $\text{AG}_5\text{CH}_5@\text{CUNCs}$ (Figure 5C).
15
16
17 424



31
32
33
34
35
36
37
38
39
40
41 425
42
43 426 **Figure 5.** Accumulation of $\text{CH}_1@\text{CUNCs}$ and core-shell nanoparticles in the inflamed colonic
44
45 427 tissues of mice. (A) Quantitative analysis of curcumin accumulated in the healthy and inflamed
46
47 428 colon samples from colitis mice after oral administration of $\text{CAP}_1\text{AG}_4\text{CH}_5@\text{CUNCs}$. (B) Confocal
48
49 429 images showing the accumulation of $\text{CH}_1@\text{CUNCs}$ and core-shell nanoparticles in inflamed
50
51 430 colons of colitis mice. The fluorescent signals of core-shell nanoparticles are shown in green
52
53 431 (white arrows). (C) Schematic illustration showing the adhesion and accumulation of
54
55
56
57
58
59
60

1
2
3 432 CAP₁AG₄CH₅@CUNCs in inflamed colons of colitis mice after oral administration. Data are
4
5 433 represented as means ± SD ($n = 6$, *** $p < 0.001$ versus healthy colon).
6
7

8 434

9
10 435 **Macroscopic grading of colitis**
11

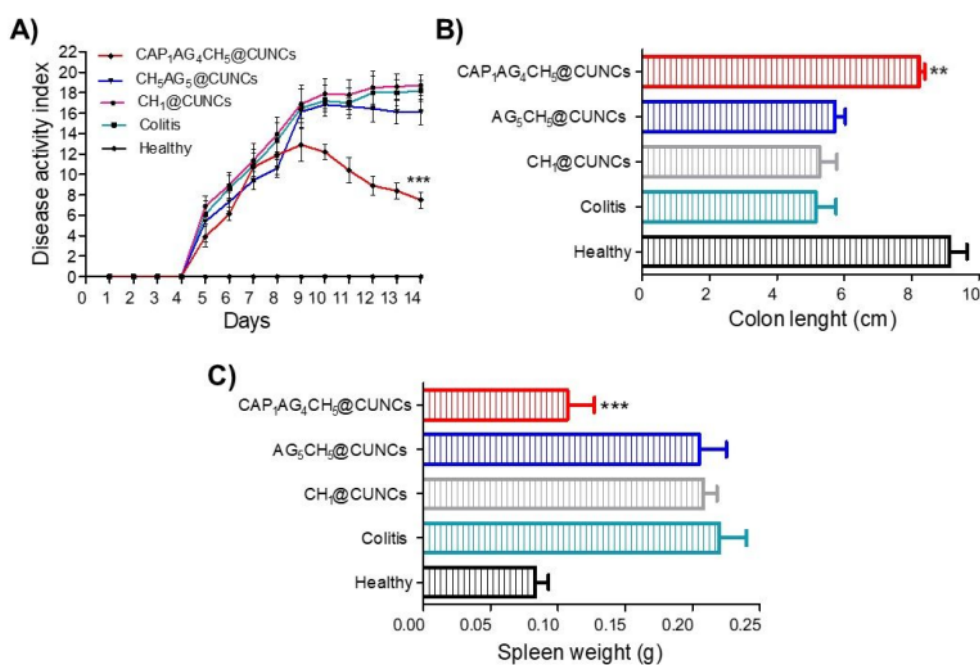
12 436

13
14 437 The DAI results indicating the severity of colitis in all studied mice groups are shown in Figure
15
16
17 438 6A. Mice in the healthy group showed constant DAI values throughout the study period, whereas
18
19 439 increased DAI (up to 18 %) was recorded in the untreated colitis mice, indicating high colitis
20
21 440 severity. Mice treated with CH₁@CUNCs and AG₅CH₅@CUNCs showed an increase in DAI by
22
23 441 (~ 18 % and ~ 16 %, respectively), indicating high colitis severity. In contrast, mice treated with
24
25 442 CAP₁AG₄CH₅@CUNCs showed significantly ($p < 0.001$) lower DAI than the untreated colitis
26
27 443 mice, indicating a lower severity of colitis.
28

29
30 444 Further, the length of the colon in mice was measured to evaluate the severity of colitis at the
31
32
33 445 end of the study (Figure 6B). The length of colon in mice in the healthy group was found to be ~
34
35 446 9 cm. In mice treated with CH₁@CUNCs and AG₅CH₅@CUNCs, colon length was markedly
36
37 447 shortened, similar to that in the colitis group (~ 5.2 and ~ 5.7 cm, respectively), indicating high
38
39 448 colitis severity. In contrast, the colon length in mice treated with CAP₁AG₄CH₅@CUNCs, was
40
41 449 found to be ~ 8.4 cm, which was significantly ($p < 0.01$) higher than that in untreated colitis mice,
42
43 450 indicating low colitis severity in the CAP₁AG₄CH₅@CUNCs-treated group. Further, we recorded
44
45 451 the spleen weight in mice as a macroscopic feature to analyze colitis severity (Figure 6C). An
46
47 452 enlarged spleen is considered to be an important indicator of the extent of inflammation in colitis.⁹
48
49 453 The spleen weight in healthy mice was ~ 0.083 ± 0.01 g, whereas, for untreated colitis mice it was
50
51 454 ~ 0.221 ± 0.02 g, indicating severe colitis. The average spleen weight in CAP₁AG₄CH₅@CUNCs-
52
53
54
55
56
57
58
59
60

1
2
3 455 treated mice was $\sim 0.107 \pm 0.02$ g, which was significantly ($p < 0.001$) lower than that of the
4
5 456 untreated colitis mice. The spleen weight in $\text{CH}_1@\text{CUNCs}$ and $\text{AG}_5\text{CH}_5@\text{CUNCs}$ -treated mice
6
7 457 was recorded to be 0.208 ± 0.01 g and 0.205 ± 0.02 g, respectively, which was similar to that in
8
9 458 the untreated colitis mice. It is worth to noting that a suspension of free curcumin was also used to
10
11 459 treat colitis mice as a separated study group. However, mice treated with free curcumin did not
12
13 460 show any significant macroscopic improvement in colitis signs (lower DAI, shorter colon length
14
15 461 and smaller spleen weight) as compared to untreated colitis mice (Figure S1).
16
17
18
19
20
21
22

462



463

464 **Figure 6.** Macroscopic analysis of colitis in mice of all experimental groups. (A) Disease activity
465 index. (B) Colon length. (C) Spleen weight. Data are presented as means \pm SD ($n = 6$, ** $p < 0.01$
466 and *** $p < 0.001$ versus colitis group).
467

467

1
2
3
4
5
6
7
8
9
10
11
12
13
14
15
16
17
18
19
20
21
22
23
24
25
26
27
28
29
30
31
32
33
34
35
36
37
38
39
40
41
42
43
44
45
46
47
48
49
50
51
52
53
54
55
56
57
58
59
60

468 **Histological analysis of colitis**

469

470 The representative images of mice colon tissue sections stained with H&E from different
471 treatment groups are shown in Figure 7A. The colon sections in healthy mice showed intact mucosa
472 without any signs of mucosal inflammation, i.e., intact epithelium, absence of edema, and no
473 infiltration of inflammatory cells, neutrophils, and macrophages. In contrast, the colonic sections
474 of untreated colitis mice showed severe histological signs of mucosal inflammation, i.e., damaged
475 epithelium, edema and infiltration of neutrophils and macrophages to the mucosa. Further, in mice
476 treated with CH₁@CUNCs and AG₅CH₅@CUNCs, no pronounced improvements in the
477 histological features of colitis were observed. As expected, the severe histological features of
478 colitis were remarkably improved by treating mice with CAP₁AG₄CH₅@CUNCs. As shown in
479 Figure 7A, re-epithelization of mucosa, absence of edema and low rate of neutrophil and
480 macrophage infiltration to the mucosa were observed in mice treated with
481 CAP₁AG₄CH₅@CUNCs. Mice treated with free curcumin did not significantly improve the
482 histological features of colitis (Figure S2).

483

484 **Immunofluorescence in mice colon**

485

486 The representative images of colon sections stained for neutrophil and macrophage infiltrations
487 using immunofluorescence are shown in Figure 7B and C, respectively. The colon sections from
488 healthy mice showed no signs of neutrophil and macrophage infiltrations to the mucosa, indicating
489 absence of colitis. However, in the colon sections from untreated colitis mice, neutrophil and
490 macrophage infiltration to mucosa was observed, indicating severe colitis. The colon sections of

1
2
3 491 mice treated with CH₁@CUNCs and AG₅CH₅@CUNCs also showed increased neutrophil and
4
5 492 macrophage infiltration, similar to that observed in untreated colitis mice. In contrast, treatment of
6
7 493 mice with CAP₁AG₄CH₅@CUNCs, largely reduced the neutrophil and macrophage infiltration to
8
9 494 mucosa, indicating improvement in severity of colitis. Free curcumin treatment did not
10
11 495 significantly reduce the neutrophil and macrophage infiltration to mucosa as compared to untreated
12
13 496 colitis mice (Figure S2).
14
15
16

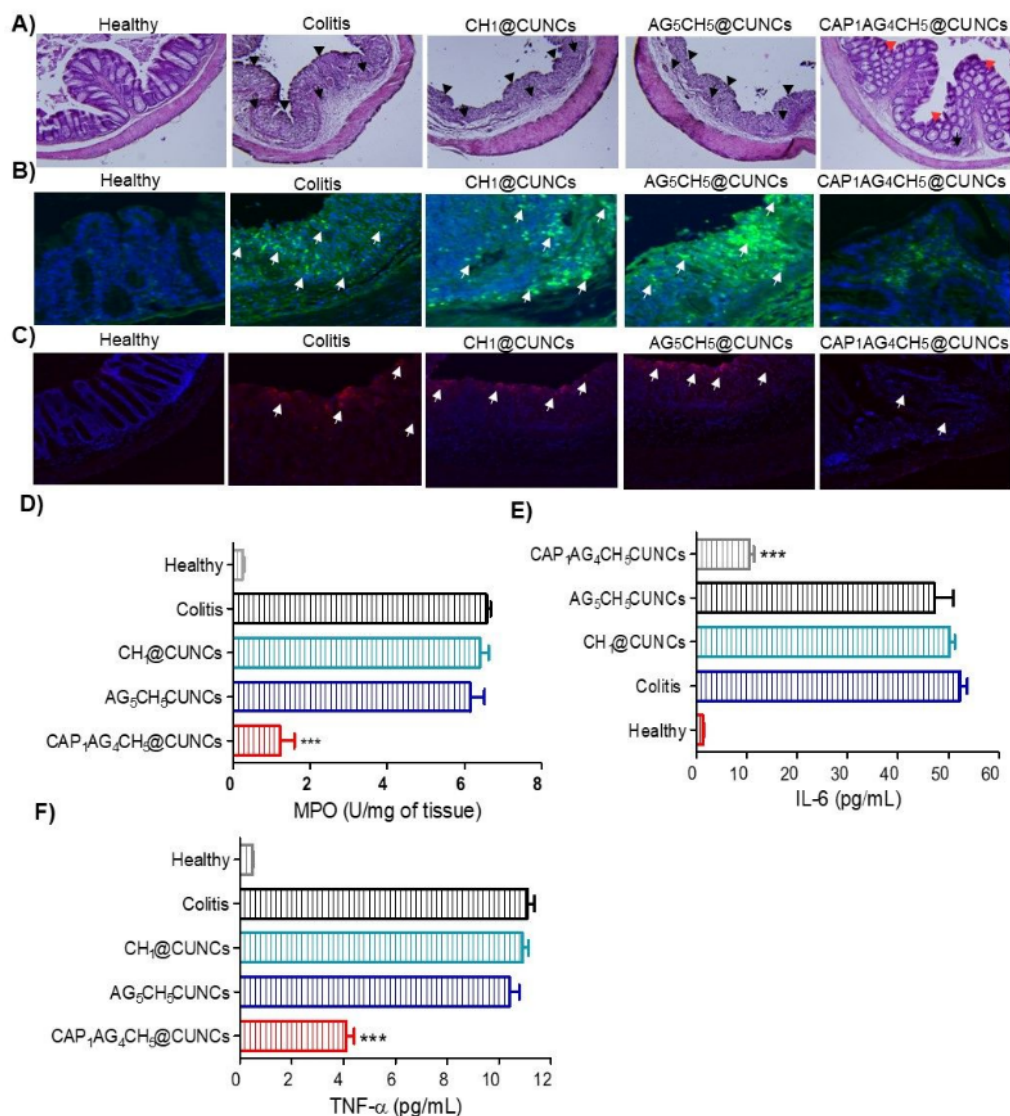
17 497 18 19 498 **Measurement of MPO activity and pro-inflammatory cytokine levels**

20
21 499 MPO is considered as an important marker for detecting neutrophil infiltration to mucosa as
22
23 500 well as degree of colitis severity.⁴³ Hence, we measured MPO activity in colon samples of all mice
24
25 501 groups. The results indicated that all mice groups except the healthy mice exhibited variable MPO
26
27 502 activities, indicating neutrophil infiltration. However, MPO activity was found to be significantly
28
29 503 lower ($p < 0.001$) in the colon of mice treated with CAP₁AG₄CH₅@CUNCs than that in untreated
30
31 504 colitis mice (Figure 7D).
32
33
34

35 505 We further confirmed the low neutrophil and macrophage infiltration in the colon samples of
36
37 506 mice treated with CAP₁AG₄CH₅@CUNCs by determining TNF- α and IL-6 levels (Figure 7E and
38
39 507 F). TNF- α and IL-6 are secreted by neutrophils and macrophages and two important inflammatory
40
41 508 mediators associated with UC pathogenesis.⁴⁴ The levels of TNF- α and IL-6 in the colon samples
42
43 509 were found to be increased in response to the induction of colitis in mice, whereas, they were
44
45 510 shown to be significantly reduced ($p < 0.001$) after CAP₁AG₄CH₅@CUNCs treatment. The
46
47 511 treatment with CH₁@CUNCs and AG₅CH₅@CUNCs did not result in any significant reduction in
48
49 512 TNF- α and IL-6 levels when compared to that in untreated colitis mice (Figure 7E and F). Free
50
51
52
53
54
55
56
57
58
59
60

1
2
3 513 curcumin treatment did not significantly reduce the MPO activity and ¹TNF- α and IL-6
4
5 514 concentrations as compared to untreated colitis mice (Figure S3).
6
7

8 515
9



50 516

51
52 517 **Figure 7.** Histological analysis of colitis in mice of all experimental groups. (A) H&E-stained
53
54 518 mice colon sections illustrate the histological changes of colitis (arrowheads, damaged epithelium;
55
56
57
58
59
60

1
2
3 519 black arrows, inflammatory cells; red arrows, re-epithelization). (B) Immunostained colon sections
4
5 520 illustrate neutrophil infiltration into mucosa (white arrows). Green, neutrophils; Blue, DAPI for
6
7 521 nuclear staining. (C) Immunostained colon sections illustrate macrophage infiltration into mucosa
8
9 522 (white arrows). Red, macrophages (F4/80); Blue, DAPI for nuclear staining. (D) MPO activity in
10
11 523 the colon samples. (E) IL-6 concentration in the colon samples. (F) TNF- α concentration in the
12
13 524 colon samples. Data are presented as means \pm SD ($n = 6$, *** $p < 0.001$ versus colitis group).
14
15
16
17 525

19 526 **DISCUSSION**

20
21 527
22
23
24 528 Core-shell nanoparticles were successfully prepared using an ultrasound-assisted antisolvent
25
26 529 crystallization and LBL-coating techniques (Figure 1A).^{27, 28} CH aqueous solution (antisolvent)
27
28 530 was gradually added to curcumin in ethanol solution (solvent) and sonicated to fabricate drug
29
30 531 nanocrystals and then coat with CH. Curcumin is a highly hydrophobic drug,⁴⁵ and tend to self-
31
32 532 aggregate in the solution during the preparation of curcumin nanoparticles.⁴⁶ The aggregated
33
34 533 nanocrystals do not represent suitable particle core for LBL-coating.²³ Hence, to prevent curcumin
35
36 534 aggregation and prepare stable drug nanocrystals, important processing conditions and formulation
37
38 535 parameters involved in the preparation were screened and optimized.⁴⁷ We found that using 2
39
40 536 mg/mL of CH aqueous solution as antisolvent with curcumin prepared in ethanol resulted in stable
41
42 537 drug nanocrystals after sonication at 150 W/cm² for 30 min. The drug nanocrystals
43
44 538 (CH₁@CUNCs) were characterized for their particle size, PDI, surface charge and shape. The
45
46 539 results showed that CH₁@CUNCs had an average size of 412 nm and positive surface charge of +
47
48 540 30 mV (Table. 1). Together, these results show that stable CH₁@CUNCs were produced and have
49
50 541 suitable core for LBL-coating with the PE, CH and AG.
51
52
53
54
55
56
57
58
59
60

1
2
3
4 542 In UC therapy, a pH-sensitive polymer coating approach of nanoparticles showed early drug
5
6 543 release by the nanoparticles in the upper GIT. This will result in reduced concentration of the drug
7
8 544 available in colon, subsequently reducing the drug efficacy.^{48, 49} In this study, we developed core-
9
10 545 shell nanoparticle forms (CAP₁AG₄CH₅@CUNCs) that reduce the drug (curcumin) leakage in the
11
12 546 upper GIT and delivers it specifically to the inflamed colon, thus decreasing the symptoms of
13
14 547 experimental colitis in mice. To control curcumin leakage from CAP₁AG₄CH₅@CUNCs during
15
16 548 their passage through the upper GIT, the CUNCs cores ¹were coated with multiple layers of CH
17
18 549 and AG followed by CAP. CH and AG are non-toxic biopolymers with good biodegradability and
19
20 550 biocompatibility profiles. Both polymers have been widely used as carriers in colon-targeted
21
22 551 nanoparticles.⁵⁰ CAP is a pH-sensitive polymer which is insoluble in the stomach pH while
23
24 552 dissolving in the colonic pH. Hence, CAP was used as an enteric coating material to resist acid
25
26 553 dissolution in the stomach and small intestine and deliver the drug to the colon.^{51, 52} The bio-
27
28 554 distribution and confocal microscopy imaging studies indicated that CAP₁AG₄CH₅@CUNCs were
29
30
31 555 highly distributed in the colon than in the upper GIT tract after oral administration in mice.
32
33
34

35 556 Despite the significant advances in UC therapy, absence of nanoparticle accumulation in the
36
37 557 inflamed tissues remains an issue. Recently, in our lab a new approach for enhancing the
38
39 558 accumulation of nanoparticles in the inflamed colonic tissues was studied for UC therapy. This
40
41 559 approach utilizes the pathophysiological changes occurring in the inflamed tissues, such as
42
43 560 elevated levels of mucus production and mucosal disruption to promote higher accumulation of
44
45 561 nanoparticles.⁹ In our study, the quantitative analysis of curcumin concentration in colon samples
46
47 562 confirmed significantly higher accumulation of CAP₁AG₄CH₅@CUNCs in the inflamed tissues
48
49 563 than the healthy ones (Figure 5A). Moreover, the confocal microscopy images of colon samples
50
51 564 showed enhanced accumulation of CAP₁AG₄CH₅@CUNCs into the inflamed colonic tissues
52
53
54
55
56
57
58
59
60

1
2
3 565 (Figure 5B). The higher accumulation could be attributed to the ability of CAP₁AG₄CH₅@CUNCs
4
5
6 566 to maintain CUNCs cores without getting dissolved in the upper GIT. Further, upon reaching the
7
8 567 colon, the nanoparticles get passively accumulated in the inflamed tissues by enhanced
9
10 568 permeability and retention effect depending on their particle size.^{9, 49, 53} Additionally the surface
11
12 569 charge-reversing property of CAP₁AG₄CH₅@CUNCs (Figure 5C) further enhances their
13
14 570 accumulation into the inflamed colons.

16
17 571 Curcumin, a major polyphenolic compound obtained from turmeric, has already ⁴been studied
18
19 572 as an anti-inflammatory agent for the treatment of UC. It regulates the inflammatory responses by
20
21 573 blocking the migration of innate immune cells, such as neutrophils and macrophages, from the
22
23 574 peripheral circulation to mucosal inflammatory sites.^{54, 55} Importantly, curcumin was ⁴recognized
24
25 575 as a safe food additive by the US Food and Drug Administration.⁵⁶ However, when it was used ⁴
26
27 576 orally in clinical trials, weak therapeutic effects were observed due to the inefficient drug delivery
28
29 577 into the inflamed colon tissues.⁴⁵ A study by Xiao et al., has used micro/nanoparticle-drug delivery
30
31 578 approach to overcome this issue in experimental murine colitis. However, the approach required
32
33 579 high dose of curcumin (50 mg/kg/day) to treat colitis.⁵⁷ In our study, we proposed a simple and
34
35 580 effective method of curcumin formulation using core-shell nanoparticles for the treatment of UC.
36
37 581 Our results indicated that a lower dose of curcumin (15 mg/kg/day) is required to treat murine
38
39 582 colitis, indicating enhanced drug potency. This is possible due to the colon-targeted delivery of
40
41 583 CAP₁AG₄CH₅@CUNCs and its high accumulation into the inflamed tissues.
42
43
44
45
46
47 584

585 CONCLUSIONS

586
59
60

1
2
3 587 In this study, colon-targeted core-shell nanoparticles were developed using CUNCs as cores
4
5 588 and pH-responsive polyelectrolyte multilayers of CH/AG/CAP as shells
6
7 589 (CAP₁AG₄CH₅@CUNCs), which can specifically deliver the drug into the inflamed colon of UC.
8
9 590 The ⁹ *in vitro* release studies showed pH-dependent release of curcumin from
10
11 591 CAP₁AG₄CH₅@CUNCs. In addition, the bio-distribution studies showed high colonic distribution
12
13 592 of CAP₁AG₄CH₅@CUNCs in mice. Further, the quantitative analysis of the drug concentration in
14
15 593 colonic tissues and confocal imaging of colons revealed that CAP₁AG₄CH₅@CUNCs were
16
17 594 preferentially adhered and accumulated in inflamed colons rather than in healthy tissues.
18
19 595 CAP₁AG₄CH₅@CUNCs showed enhanced therapeutic efficacy at treating DSS-induced colitis in
20
21 596 mice. Overall, the drug ⁴ delivery system developed in the current study has great potential for
22
23 597 application in colon-targeted UC therapy.
24
25
26
27
28
29
30

31 599 SUPPORTING INFORMATION

32
33 600 Methodology on drug loading; Statistical analysis; Physicochemical characteristics of core-shell
34
35 601 nanoparticles with shells having ¹ different numbers of CH/AG/CAP multilayers; Macroscopic
36
37 602 analysis of colitis; Histological analysis of colitis and immunostaining of colonic tissues; ¹⁰ MPO
38
39 603 activity and pro-inflammatory cytokine levels
40
41
42
43
44

45 605 AUTHOR INFORMATION

46 606 Corresponding Author

47 607 Jin-Wook Yoo

48 608 College of Pharmacy, Pusan National University, Busandaehak-ro 63 beon-gil, Geumjeong-gu,
49 609 Busan, South Korea.

1
2
3 610 Tel: +82-51-510-2807
4
5 611 Fax: +82 51 513 6754
6
7
8 612 E-mail: jinwook@pusan.ac.kr
9

10 613

11
12 614 **NOTE**

13
14 **1**
15 615 There is no conflict of interest to declare in this study.

16
17 616

18
19 617 **ACKNOWLEDGMENTS**

20
21 618 This research was supported by the Basic Science Research Program through the National
22
23 619 Research Foundation of Korea (NRF) funded by the Ministry of Education (grant number: NRF-
24
25 620 2019R111A3A01057849).
26
27

28
29 621

30
31 622 **REFERENCES**

- 32
33 623 1. Danese, S.; Fiocchi, C. Ulcerative colitis. *N. Engl. J. Med.* **2011**, 365, (18), 1713-
34
35 624 1725.
36
37 625 2. Oshi, M. A.; Naeem, M.; Bae, J.; Kim, J.; Lee, J.; Hasan, N.; Kim, W.; Im, E.; Jung,
38
39 626 Y.; Yoo, J.-W. Colon-targeted dexamethasone microcrystals with pH-sensitive
40
41 627 chitosan/alginate/Eudragit S multilayers for the treatment of inflammatory bowel
42
43 628 disease. *Carbohydr. Polym.* **2018**, 198, 434-442.
44
45 629 3. Kenyon, C. J.; Nardi, R. V.; Wong, D.; Hooper, G.; Wilding, I. R.; Friend, D. R. Colonic
46
47 630 delivery of dexamethasone: a pharmacoscintigraphic evaluation. *Aliment. Pharmacol.*
48
49 631 *Ther. Symp. Ser.* **1997**, 11, (1), 205-213.
50
51
52
53
54
55
56
57
58
59
60

- 1
2
3 632 4. Naeem, M.; Awan, U. A.; Subhan, F.; Cao, J.; Hlaing, S. P.; Lee, J.; Im, E.; Jung, Y.;
4
5 633 Yoo, J.-W. Advances in colon-targeted nano-drug delivery systems: challenges and
6
7 634 solutions. *Arch. Pharmacol Res.* **2020**, 43, (1), 153-169.
8
9
10 635 5. Zhang, M.; Merlin, D. Nanoparticle-based oral drug delivery systems targeting the
11
12 636 colon for treatment of ulcerative colitis. *Inflammatory Bowel Dis.* **2018**, 24, (7), 1401-
13
14 637 1415.
15
16 638 6. Thapaliya, R.; Shrestha, K.; Sharma, A.; Dhakal, N.; Manandhar, P.; Shrestha, S.;
17
18 639 Bhattarai, R. Physicochemical characterization of naproxen microcrystals for colon
19
20 640 specific pulsatile drug delivery designed using pulsincap technique. *J. Pharm. Invest.*
21
22 641 **2019**, 49, (5), 553-564.
23
24 642 7. Kumar, J.; Newton, A. M. Rifaximin - chitosan nanoparticles for inflammatory bowel
25
26 643 disease (IBD). *Recent Pat. Inflammation Allergy Drug Discovery* **2017**, 11, (1), 41-52.
27
28 644 8. Davoudi, Z.; Peroutka-Bigus, N.; Bellaire, B.; Wannemuehler, M.; Barrett, T. A.;
29
30 645 Narasimhan, B.; Wang, Q. Intestinal organoids containing poly(lactic-co-glycolic acid)
31
32 646 nanoparticles for the treatment of inflammatory bowel diseases. *J. Biomed. Mater.*
33
34 647 *Res., Part A* **2018**, 106, (4), 876-886.
35
36 648 9. Naeem, M.; Oshi, M. A.; Kim, J.; Lee, J.; Cao, J.; Nurhasni, H.; Im, E.; Jung, Y.; Yoo,
37
38 649 J.-W. pH-triggered surface charge-reversal nanoparticles alleviate experimental
39
40 650 murine colitis via selective accumulation in inflamed colon regions. *Nanomed-*
41
42 651 *nanotechnol.* **2018**, 14, (3), 823-834.
43
44 652 10. Ferri, D.; Gaviña, P.; Parra, M.; Costero, A. M.; El Haskouri, J.; Amorós, P.; Merino,
45
46 653 V.; Teruel, A. H.; Sancenón, F.; Martínez-Máñez, R. Mesoporous silica microparticles
47
48
49
50
51
52
53
54
55
56
57
58
59
60

- 1
2
3 654 gated with a bulky azo derivative for the controlled release of dyes/drugs in colon. *R.*
4
5 655 *Soc. Open Sci.* **2018**, 5, (8), 180873-180877.
6
7
8 656 11. Gupta, A. S.; Kshirsagar, S. J.; Bhalekar, M. R.; Saldanha, T. Design and
9
10 657 development of liposomes for colon targeted drug delivery. *J. Drug Targeting* **2013**,
11
12 658 21, (2), 146-160.
13
14 659 12. Han, S.-M.; Na, Y.-G.; Lee, H.-S.; Son, G.-H.; Jeon, S.-H.; Bang, K.-H.; Kim, S.-J.;
15
16 660 Lee, H.-J.; Cho, C.-W. Improvement of cellular uptake of hydrophilic molecule,
17
18 661 calcein, formulated by liposome. *J. Pharm. Invest.* **2018**, 48, (5), 595-601.
19
20
21 662 13. Ma, Y.; Fuchs, A. V.; Boase, N. R. B.; Rolfe, B. E.; Coombes, A. G. A.; Thurecht, K.
22
23 663 J. The in vivo fate of nanoparticles and nanoparticle-loaded microcapsules after oral
24
25 664 administration in mice: Evaluation of their potential for colon-specific delivery. *Eur. J.*
26
27 665 *Pharm. Biopharm.* **2015**, 94, 393-403.
28
29
30 666 14. Knipe, J. M.; Strong, L. E.; Peppas, N. A. Enzyme- and pH-responsive
31
32 667 microencapsulated nanogels for oral delivery of siRNA to induce TNF- α
33
34 668 knockdown in the intestine. *Biomacromolecules* **2016**, 17, (3), 788-797.
35
36
37 669 15. Zhang, M.; Viennois, E.; Xu, C.; Merlin, D. Plant derived edible nanoparticles as a
38
39 670 new therapeutic approach against diseases. *Tissue Barriers* **2016**, 4, (2), e1134415-
40
41 671 e1134415.
42
43
44 672 16. Agarwal, A.; Lvov, Y.; Sawant, R.; Torchilin, V. Stable nanocolloids of poorly soluble
45
46 673 drugs with high drug content prepared using the combination of sonication and layer-
47
48 674 by-layer technology. *J. Controlled Release* **2008**, 128, (3), 255-260.
49
50
51
52
53
54
55
56
57
58
59
60

- 1
2
3 675 17. Rostami, M.; Zamani, R. M.; Aghajanzadeh, K. M.; Danafar, H. Sol-gel synthesis and
4
5 676 characterization of zinc ferrite-graphene nano-hybrids for photo-catalytic degradation
6
7 677 of the paracetamol. *J. Pharm. Invest.* **2018**, 48, (6), 657-664.
8
9
10 678 18. Sharma, S.; Verma, A.; Teja, B. V.; Shukla, P.; Mishra, P. R. Development of
11
12 679 stabilized Paclitaxel nanocrystals: In-vitro and in-vivo efficacy studies. *Eur. J. Pharm.*
13
14 680 *Sci.* **2015**, 69, 51-60.
15
16
17 681 19. Singh, D.; Bedi, N.; Tiwary, A. K. Enhancing solubility of poorly aqueous soluble
18
19 682 drugs: critical appraisal of techniques. *J. Pharm. Invest.* **2018**, 48, (5), 509-526.
20
21 683 20. Kawabata, Y.; Wada, K.; Nakatani, M.; Yamada, S.; Onoue, S. Formulation design
22
23 684 for poorly water-soluble drugs based on biopharmaceutics classification system:
24
25 685 Basic approaches and practical applications. *Int. J. Pharm.* **2011**, 420, (1), 1-10.
26
27
28 686 21. Van Hoogevest, P.; Liu, X.; Fahr, A. Drug delivery strategies for poorly water-soluble
29
30 687 drugs: the industrial perspective. *Expert Opin. Drug Delivery* **2011**, 8, (11), 1481-500.
31
32
33 688 22. Fuhrmann, K.; Polomska, A.; Aeberli, C.; Castagner, B.; Gauthier, M. A.; Leroux, J.
34
35 689 C. Modular design of redox-responsive stabilizers for nanocrystals. *ACS Nano* **2013**,
36
37 690 7, (9), 8243-8250.
38
39
40 691 23. Polomska, A.; Gauthier, M. A.; Leroux, J. C. In vitro and in vivo evaluation of
41
42 692 PEGylated layer-by-layer polyelectrolyte-coated paclitaxel nanocrystals. *Small* **2017**,
43
44 693 13, (2), 1-12.
45
46
47 694 24. Deshpande, S.; Sharma, S.; Koul, V.; Singh, N. Core-shell nanoparticles as an
48
49 695 efficient, sustained, and triggered drug-delivery system. *ACS Omega* **2017**, 2, (10),
50
51 696 6455-6463.
52
53
54
55
56
57
58
59
60

- 1
2
3 697 25. Ghosh Chaudhuri, R.; Paria, S. Core/shell nanoparticles: classes, properties,
4
5 698 synthesis mechanisms, characterization, and applications. *Chem. Rev.* **2011**, 112,
6
7 699 (4), 2373-2433.
8
9
10 700 26. Wanawananon, K.; Moulton, S. E.; Wallace, G. G.; Liawruangrath, S. Fabrication of
11
12 701 novel core-shell PLGA and alginate fiber for dual-drug delivery system. *Polym. Adv.*
13
14 702 *Technol.* **2016**, 27, (8), 1014-1019.
15
16
17 703 27. Park, M.-W.; Yeo, S.-D. Antisolvent crystallization of roxithromycin and the effect of
18
19 704 ultrasound. *Polym. Adv. Technol.* **2010**, 45, (10), 1402-1410.
20
21
22 705 28. Polomska, A.; Gauthier, M. A.; Leroux, J. C. In vitro and in vivo evaluation of
23
24 706 PEGylated layer-by-layer polyelectrolyte-coated paclitaxel nanocrystals. *Small* **2017**,
25
26 707 13, (2), 1602066.
27
28
29 708 29. Chai, F.; Sun, L.; He, X.; Li, J.; Liu, Y.; Xiong, F.; Ge, L.; Webster, T. J.; Zheng, C.
30
31 709 Doxorubicin-loaded poly (lactic-co-glycolic acid) nanoparticles coated with
32
33 710 chitosan/alginate by layer by layer technology for antitumor applications. *Int. J.*
34
35 711 *Nanomed.* **2017**, 12, 1791-1802.
36
37
38 712 30. Beloqui, A.; Coco, R.; Memvanga, P. B.; Ucakar, B.; des Rieux, A.; Preat, V. pH-
39
40 713 sensitive nanoparticles for colonic delivery of curcumin in inflammatory bowel
41
42 714 disease. *Int. J. Pharm.* **2014**, 473, (1-2), 203-212.
43
44
45 715 31. Cui, J.; Yu, B.; Zhao, Y.; Zhu, W.; Li, H.; Lou, H.; Zhai, G. Enhancement of oral
46
47 716 absorption of curcumin by self-microemulsifying drug delivery systems. *Int. J. Pharm.*
48
49 717 **2009**, 371, (1), 148-155.
50
51
52
53
54
55
56
57
58
59
60

- 1
2
3 718 32. Madhavi, M.; Madhavi, K.; Jithan, A. V. Preparation and in vitro/in vivo
4
5 719 characterization of curcumin microspheres intended to treat colon cancer. *J. Pharm.*
6
7 720 *BioAllied Sci.* **2012**, 4, (2), 164-171.
8
9
10 721 33. Zhang, J.; Liu, S.; Hu, X.; Xie, Z.; Jing, X. Cyanine-curcumin assembling
11
12 722 nanoparticles for near-infrared imaging and photothermal therapy. *ACS Biomater.*
13
14 723 *Sci. Eng.* **2016**, 2, (11), 1942-1950.
15
16
17 724 34. Cui, J.; Yu, B.; Zhao, Y.; Zhu, W.; Li, H.; Lou, H.; Zhai, G. Enhancement of oral
18
19 725 absorption of curcumin by self-microemulsifying drug delivery systems. *Int. J. Pharm.*
20
21 726 **2009**, 371, (1-2), 148-55.
22
23
24 727 35. Hartmann, G.; Bidlingmaier, C.; Siegmund, B.; Albrich, S.; Schulze, J.; Tschoep, K.;
25
26 728 Eigler, A.; Lehr, H. A.; Endres, S. Specific type IV phosphodiesterase inhibitor
27
28 729 rolipram mitigates experimental colitis in mice. *J. Pharmacol. Exp. Ther.* **2000**, 292,
29
30 730 (1), 22-30.
31
32
33 731 36. Viennois, E.; Xiao, B.; Ayyadurai, S.; Wang, L.; Wang, P. G.; Zhang, Q.; Chen, Y.;
34
35 732 Merlin, D. Micheliolide, a new sesquiterpene lactone that inhibits intestinal
36
37 733 inflammation and colitis-associated cancer. *Lab. Invest.* **2014**, 94, 950.
38
39
40 734 37. Weigmann, B.; Lehr, H. A.; Yancopoulos, G.; Valenzuela, D.; Murphy, A.; Stevens,
41
42 735 S.; Schmidt, J.; Galle, P. R.; Rose-John, S.; Neurath, M. F. The transcription factor
43
44 736 NFATc2 controls IL-6-dependent T cell activation in experimental colitis. *J. Exp. Med.*
45
46 737 **2008**, 205, (9), 2099-2110.
47
48
49 738 38. Naeem, M.; Bae, J.; Oshi, M. A.; Kim, M.-s.; Moon, H. R.; Lee, B. L.; Im, E.; Jung, Y.;
50
51 739 Yoo, J.-W. Colon-targeted delivery of cyclosporine A using dual-functional Eudragit®
52
53
54
55
56
57
58
59
60

- 1
2
3 740 FS30D/PLGA nanoparticles ameliorates murine experimental colitis. *Int. J. Nanomed.*
4
5 741 **2018**, 13, 1225-1230.
6
7
8 742 39. Kim, J. J.; Shajib, M. S.; Manocha, M. M.; Khan, W. I. Investigating intestinal
9
10 743 inflammation in DSS-induced model of IBD. *J. Visualized Exp.* **2012**, (60), 3678
11
12 744 40. Wan, S.; Sun, Y.; Qi, X.; Tan, F. Improved bioavailability of poorly water-soluble drug
13
14 745 curcumin in cellulose acetate solid dispersion. *AAPS PharmSciTech* **2012**, 13, (1),
15
16 746 159-166.
17
18
19 747 41. Park, S. C.; Kim, M. J.; Choi, K.; Kim, J.; Choi, S.-O. Influence of shell compositions
20
21 748 of solution blown PVP/PCL core-shell fibers on drug release and cell growth. *RSC*
22
23 749 *Adv.* **2018**, 8, (57), 32470-32480.
24
25
26 750 42. Santos, A. C.; Pattekari, P.; Jesus, S.; Veiga, F.; Lvov, Y.; Ribeiro, A. J. Sonication-
27
28 751 assisted layer-by-layer assembly for low solubility drug nanoformulation. *ACS Appl.*
29
30 752 *Mater. Interfaces* **2015**, 7, (22), 11972-11983.
31
32
33 753 43. Mendoza, J. L.; Abreu, M. T. Biological markers in inflammatory bowel disease:
34
35 754 Practical consideration for clinicians. *Gastroenterol. Clin. Biol.* **2009**, 33, (Supplement
36
37 755 3), S158-S173.
38
39
40 756 44. Poh, S.; Lin, J. B.; Panitch, A. Release of anti-inflammatory peptides from
41
42 757 thermosensitive nanoparticles with degradable cross-links suppresses pro-
43
44 758 inflammatory cytokine production. *Biomacromolecules* **2015**, 16, (4), 1191-1200.
45
46
47 759 45. Anand, P.; Kunnumakkara, A. B.; Newman, R. A.; Aggarwal, B. B. Bioavailability of
48
49 760 curcumin: problems and promises. *Mol. Pharmaceutics* **2007**, 4, (6), 807-818.
50
51
52
53
54
55
56
57
58
59
60

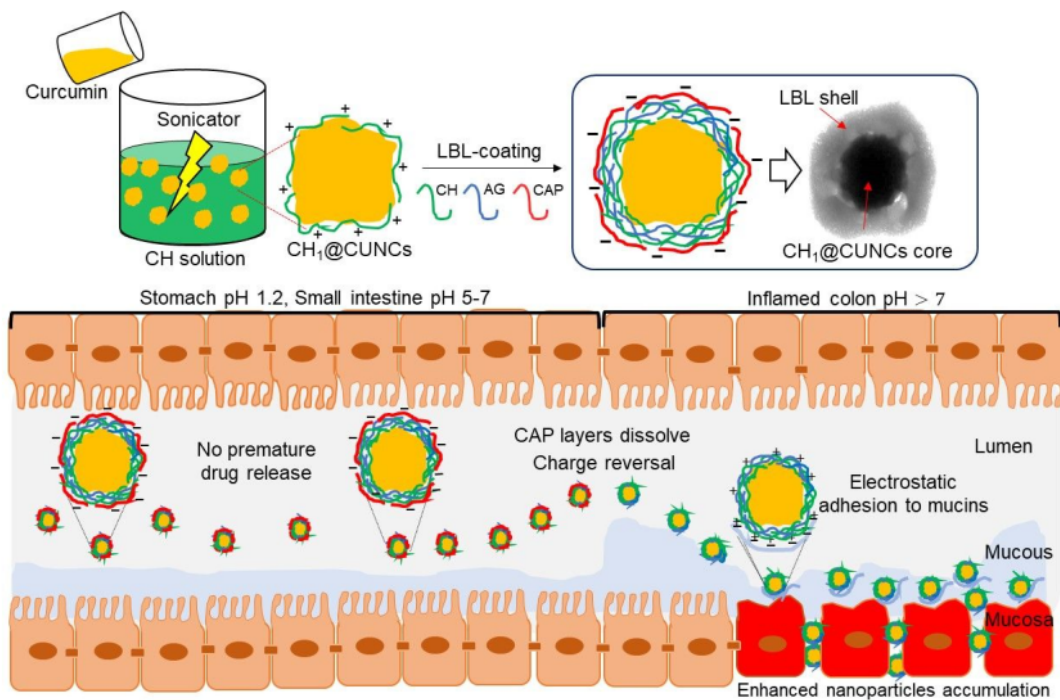
- 1
2
3 761 46. Moorthi, C.; Krishnan, K.; Manavalan, R.; Kathiresan, K. Preparation and
4
5 762 characterization of curcumin-piperine dual drug loaded nanoparticles. *Asian Pac. J.*
6
7 763 *Trop. Biomed.* **2012**, 2, (11), 841-848.
8
9
10 764 47. Iurian, S.; TomuȚA, I.; Rus, L.; Achim, M.; Leucuta, S. E. Optimization of the
11
12 765 sonication process for meloxicam nanocrystals preparation. *Clujul Med.* **2015**, 88, (3),
13
14 766 366-372.
15
16
17 767 48. Lamprecht, A.; Ubrich, N.; Yamamoto, H.; Schäfer, U.; Takeuchi, H.; Lehr, C.-M.;
18
19 768 Maincent, P.; Kawashima, Y. J. Design of rolipram-loaded nanoparticles: comparison
20
21 769 of two preparation methods. *J. Controlled Release* **2001**, 71, (3), 297-306.
22
23
24 770 49. Lamprecht, A.; Ubrich, N.; Yamamoto, H.; Schäfer, U.; Takeuchi, H.; Maincent, P.;
25
26 771 Kawashima, Y.; Lehr, C.-M. Biodegradable nanoparticles for targeted drug delivery
27
28 772 in treatment of inflammatory bowel disease. *J. Pharmacol. Exp. Ther.* **2001**, 299, (2),
29
30 773 775-781.
31
32
33 774 50. Chourasia, M. K; Jain, S. K. Polysaccharides for colon targeted drug delivery. *Drug*
34
35 775 *Delivery* **2004**, 11, (2), 129-148.
36
37
38 776 51. Ganguly, K.; Aminabhavi, T. M.; Kulkarni, A. R. Colon targeting of 5-fluorouracil using
39
40 777 polyethylene glycol cross-linked chitosan microspheres enteric coated with cellulose
41
42 778 acetate phthalate. *Ind. Eng. Chem. Res.* **2011**, 50, (21), 11797-11807.
43
44
45 779 52. Levine, D. S.; Raisys, V. A.; Ainardi, V. Coating of oral beclomethasone dipropionate
46
47 780 capsules with cellulose acetate phthalate enhances delivery of topically active
48
49 781 antiinflammatory drug to the terminal ileum. *Gastroenterology* **1987**, 92, (4), 1037-
50
51 782 1044.
52
53
54
55
56
57
58
59
60

- 1
2
3 783 53. Lamprecht, A.; Schafer, U.; Lehr, C. M. Size-dependent bioadhesion of micro- and
4
5 784 nanoparticulate carriers to the inflamed colonic mucosa. *Pharm. Res.* **2001**, 18, (6),
6
7 785 788-793.
8
9
10 786 54. Ukil, A.; Maity, S.; Karmakar, S.; Datta, N.; Vedasiromoni, J. R.; Das, P. K. Curcumin,
11
12 787 the major component of food flavour turmeric, reduces mucosal injury in
13
14 788 trinitrobenzene sulphonic acid-induced colitis. *Br. J. Pharmacol.* **2003**, 139, (2), 209-
15
16 789 218.
17
18
19 790 55. Young, N. A.; Bruss, M. S.; Gardner, M.; Willis, W. L.; Mo, X.; Valiente, G. R.; Cao,
20
21 791 Y.; Liu, Z.; Jarjour, W. N.; Wu, L. C. Oral administration of nano-emulsion curcumin
22
23 792 in mice suppresses inflammatory-induced NFkappaB signaling and macrophage
24
25 793 migration. *PloS one* **2014**, 9, (11), e111559.
26
27
28 794 56. Clinical development plan: curcumin. *J. Cell. Biochem. Suppl.* **1996**, 26, 72-85.
29
30
31 795 57. Xiao, B.; Si, X.; Zhang, M.; Merlin, D. Oral administration of pH-sensitive curcumin-
32
33 796 loaded microparticles for ulcerative colitis therapy. *Colloids Surf., B* **2015**, 135, 379-
34
35 797 385.
36
37
38 798
39
40
41
42
43
44
45
46
47
48
49
50
51
52
53
54
55
56
57
58
59
60

799 **Table of contents graphic (TOC)**

800

801



802

ORIGINALITY REPORT

16%

SIMILARITY INDEX

10%

INTERNET SOURCES

15%

PUBLICATIONS

7%

STUDENT PAPERS

PRIMARY SOURCES

- 1 Murtada A. Oshi, Muhammad Naeem, Junhwan Bae, Jihyun Kim et al. "Colon-targeted dexamethasone microcrystals with pH-sensitive chitosan/alginate/Eudragit S multilayers for the treatment of inflammatory bowel disease", Carbohydrate Polymers, 2018
Publication 3%
- 2 jyx.jyu.fi
Internet Source 2%
- 3 Submitted to Taipei Medical University
Student Paper 2%
- 4 Shangyong Li, Mengfei Jin, Yanhong Wu, Samil Jung, Dandan Li, Ningning He, Myeong-sok Lee. "An efficient enzyme-triggered controlled release system for colon-targeted oral delivery to combat dextran sodium sulfate (DSS)-induced colitis in mice", Drug Delivery, 2021
Publication 1%
- 5 Sang Hoon Lee, Jae Geun Song, Hyo-Kyung Han. "Site-selective oral delivery of 1%

therapeutic antibodies to the inflamed colon via a folic acid-grafted organic/inorganic hybrid nanocomposite system", *Acta Pharmaceutica Sinica B*, 2022

Publication

6

Submitted to Pusan National University Library

Student Paper

1 %

7

Seongkeun Jeong, Sanghyun Ju, Sohee Park, Yunjin Jung. "5-[(3-Carboxy-4-hydroxyphenyl)diazenyl] nicotinic acid, an azo-linked mesalazine-nicotinic acid conjugate, is a colon-targeted mutual prodrug against dextran sulfate sodium-induced colitis in mice", *Journal of Pharmaceutical Investigation*, 2021

Publication

1 %

8

Zonghua Tian, Xia Wu, Li Peng, Na Yu, Guojing Gou, Wenbao Zuo, Jianhong Yang. "pH-responsive bufadienolides nanocrystals decorated by chitosan quaternary ammonium salt for treating colon cancer", *International Journal of Biological Macromolecules*, 2023

Publication

1 %

9

Yongqing Huang, Yuxin Zhou, Yao Shen, Jin Wang, Liangliang Zhou, Zhenhua Chen. "Preparation of baicalin colon-targeted

1 %

granules and its intervention effect on ulcerative colitis in rats", Particuology, 2023

Publication

10

Muhammad Naeem, Murtada A. Oshi, Jihyun Kim, Juho Lee, Jiafu Cao, Hasan Nurhasni, Eunok Im, Yunjin Jung, Jin-Wook Yoo. "pH-triggered surface charge-reversal nanoparticles alleviate experimental murine colitis via selective accumulation in inflamed colon regions", Nanomedicine: Nanotechnology, Biology and Medicine, 2018

Publication

1 %

11

Yingni Lv, Mengjiao Ren, Min Yao, Jiafeng Zou, Siqi Fang, Yanbing Wang, Minbo Lan, Yuzheng Zhao, Feng Gao. "Colon-specific delivery of methotrexate using hyaluronic acid modified pH-responsive nanocarrier for the therapy of colitis in mice", International Journal of Pharmaceutics, 2023

Publication

1 %

12

Aline Martins dos Santos, Suzana Gonçalves Carvalho, Andréia Bagliotti Meneguim, Rafael Miguel Sábio et al. "Oral delivery of micro/nanoparticulate systems based on natural polysaccharides for intestinal diseases therapy: Challenges, advances and future perspectives", Journal of Controlled Release, 2021

Publication

1 %

13

test.dovepress.com

Internet Source

1 %

14

docksci.com

Internet Source

1 %

15

Juho Lee, Murtada A Oshi, Dongmin Kwak, Hyunwoo Kim et al. "On-demand reconstitutable hyaluronic acid-doped azathioprine microcrystals effectively ameliorate ulcerative colitis via selective accumulation in inflamed tissues", Biomaterials Science, 2022

Publication

1 %

Exclude quotes On

Exclude matches < 1%

Exclude bibliography On